

Bilinear Subspace Variational Bayesian Inference for Joint Scattering Environment Sensing and Data Recovery in ISAC Systems

An Liu, *Senior Member, IEEE*, Wenkang Xu, Wei Xu, and Giuseppe Caire, *Fellow, IEEE*

Abstract—This paper considers a joint scattering environment sensing and data recovery problem in an uplink integrated sensing and communication (ISAC) system. To facilitate joint scatterers localization and multi-user (MU) channel estimation, we introduce a three-dimensional (3D) location-domain sparse channel model to capture the joint sparsity of the MU channel (i.e., different user channels share partially overlapped scatterers). Then the joint problem is formulated as a bilinear structured sparse recovery problem with a dynamic position grid and imperfect parameters (such as time offset and user position errors). We propose an expectation maximization based turbo bilinear subspace variational Bayesian inference (EM-Turbo-BiSVBI) algorithm to solve the problem effectively, where the E-step performs Bayesian estimation of the the location-domain sparse MU channel by exploiting the joint sparsity, and the M-step refines the dynamic position grid and learns the imperfect factors via gradient update. Two methods are introduced to greatly reduce the complexity with almost no sacrifice on the performance and convergence speed: 1) a subspace constrained bilinear variational Bayesian inference (VBI) method is proposed to avoid any high-dimensional matrix inverse; 2) the multiple signal classification (MUSIC) and subspace constrained VBI methods are combined to obtain a coarse estimation result to reduce the search range. Simulations verify the advantages of the proposed scheme over baseline schemes.

Index Terms—ISAC, joint sensing and data recovery, bilinear subspace variational Bayesian inference.

Then the joint problem is formulated as a bilinear structured sparse

I. INTRODUCTION

Due to the deployment of wideband orthogonal frequency division multiplexing (OFDM) waveform and massive multi-input multi-output (MIMO) technologies, communication signals in future 6G wireless systems tend to have high-resolution in both time and angular domain. Under such a background, integrated sensing and communication (ISAC), in which communication signals are exploited to simultaneously achieve high-speed communication and high-accuracy sensing, has emerged as a key technology to support many important applications [1]–[3].

There are two basic ISAC scenarios [4]: broadcast channel (BC) with mono-static sensing and multiple access channel (MAC) with bi-static sensing. In BC with mono-static sensing, the base station (BS) acts as both radar transceiver and communication transmitter. In this case, the BS knows the

An Liu, Wenkang Xu, and Wei Xu are with the College of Information Science and Electronic Engineering, Zhejiang University, Hangzhou 310027, China (email: anliu@zju.edu.cn).

G. Caire is with the Department of Telecommunication Systems, Technical University of Berlin, 10587 Berlin, Germany (e-mail: caire@tu-berlin.de).

transmit data and the sensing problem is relatively easy. In MAC with bi-static sensing, the BS acts as both radar and communication receivers, while the user acts as both radar and communication transmitters, as illustrated in Fig. 1. In this case, the challenge at BS side is how to perform joint environment sensing, channel estimation, and data recovery with only limited pilot signals and unknown transmit data, under possibly imperfect factors such as time offset between the BS and users, and position errors of users.

This paper considers the more challenging ISAC scenario of MAC with bi-static sensing. In particular, we investigate a joint scattering environment sensing and data recovery problem in the uplink of a massive MIMO-OFDM ISAC system, where the BS exploits both the uplink pilot and data signals to jointly detect/localize the scatterers in the multi-user (MU) propagation environment, estimate the uplink channels, and recover the data from all users. Some related works are reviewed below.

Joint scattering environment sensing and channel estimation: Since multiple users in the same cell share a common scattering environment, the three-dimensional (3D) scatterers seen by different users have a partially overlapping structure. The work in [5], [6] revealed that MU channels exhibit a hidden joint sparsity in the angular-domain due to the shared scattering environment, which can be exploited to enhance the channel estimation performance. [3], [7] concentrated on the partially overlapping structure between radar targets and communication scatterers, and a joint target sensing and channel estimation scheme was designed based the joint sparsity of radar and communication channels. The above works only consider the oversimplified case when MU or ISAC channels share a partially overlapping support in the angular domain, while the shared location-domain information is not fully used. A recent work in [8], [9] has proposed a two-dimensional (2D) location-domain sparse channel model to exploit the partially overlapping support of MU channels for the special case when all scatterers lies in a 2D area. However, the 3D location-domain sparse channel modeling is still not fully investigated. Moreover, the existing works perform joint scattering environment sensing and channel estimation based on pilot signals only. Nevertheless, data signals also provides much information about wireless channels that can help reduce pilot overhead.

Joint channel estimation and data recovery for pure communications: In [10], the authors developed a two-stage framework consisting of a semiblind channel estimator and a semiblind data detector, where the data detector can use

the error statistics to mitigate the effect of channel estimation error. In [11], [12], the joint problem is formulated as a bilinear observation model, and a bilinear generalized approximate message passing (BiGAMP) algorithm is developed to achieve bilinear sparse signal recovery. A turbo-like detection approach called GAMP in [13] estimated channels and data consequently and the estimation error of each phase is modeled as additional additive noise for the following one. In [14], [15], a variational Bayesian inference (VBI) algorithm was developed to obtain the posterior distribution of channels and data alternatively.

The joint sensing and data recovery problem considered in this paper is essentially a structured sparse signal recovery problem with a bilinear observation model and a dynamic grid as well as imperfect parameters. However, such a problem has not been fully investigated before, especially for the more practical scenarios of detecting and localizing the scatterers in a 3D space using both pilot and data signals, under the consideration of imperfect parameters. Clearly, the existing algorithms for joint channel estimation and data recovery cannot be easily extended to solve this problem, and there still lacks efficient algorithms that have both low complexity and theoretical performance guarantees. For example, the commonly used BiGAMP algorithm is heuristic and has no theoretical performance guarantee [11], [12]. As such, the performance is very sensitive to the properties of the observation model and fine-tuning of the algorithm parameters. It is difficult to adjust the algorithm parameters to achieve a stable performance for the complicated joint sensing and data recovery problem. The algorithm based on more rigorous theory, such as VBI [14], [15], involves high-dimensional matrix inverse. And thus, its complexity is unacceptable in practice, especially for massive MIMO-OFDM with huge dimensions of both sparse channels and observations.

In summary, the following challenges have not been fully addressed in existing works: 1) The modeling and exploitation of the partially overlapped supports of MU channels (which is referred to as joint sparsity in this paper) in the 3D location domain remains untapped. 2) For bilinear sparse signal recovery problem with both a dynamic grid and imperfect factors, there still lacks robust algorithm design with both theoretical performance guarantees and low complexity. 3) There still lacks efficient method to handle the ultra-high-dimensional sparse channel caused by the 3D sparse modeling of massive MIMO-OFDM MU channels. To overcome those challenges, we propose a joint sensing and data recovery algorithm based on a 3D location-domain sparse channel modeling and a novel bilinear subspace variational Bayesian inference (BiSVBI) algorithm. The main contributions are summarized below.

- **3D location-domain sparse channel modeling:** To fully exploit the partially overlapped structure of 3D scatterers of MU channels, we propose a 3D location-domain sparse channel representation, where the entire 3D scattering environment is partitioned into Q dynamic position grids, and the q -th element of the location-domain sparse channel vector is the channel coefficient corresponding to the scatterer located at the q -th position grid. Then, we propose a three-layer Bernoulli-Gamma-Gaussian (BGG)

prior to capture the joint sparsity of MU channels in the 3D location domain.

- **BiSVBI algorithm:** We model the joint sensing and data recovery problem as a bilinear structured sparse signal recovery problem with a dynamic grid and imperfect factors. Then, we propose an expectation maximization based turbo BiSVBI (EM-Turbo-BiSVBI) algorithm to solve this problem efficiently, where the E-step performs Bayesian estimation of the location-domain sparse channels and the M-step refines the dynamic grid and learns the imperfect factors via gradient update. In particular, the E-step is based on a novel BiSVBI algorithm by minimizing the KL-divergence (KLD) between the variational posterior distribution and the true posterior associated with the bilinear model. To reduce the complexity, an independent constraint is imposed on the variational posterior distribution of the sparse channels to avoid matrix inverse in the calculation of the posterior covariance matrix. Moreover, a subspace constrained matrix inverse followed by a gradient update is proposed to replace the high dimensional matrix inverse in the calculation of the posterior mean. Theoretical analysis and simulations show that BiSVBI greatly reduces the algorithm complexity with almost no sacrifice on the performance and convergence speed.

- **Coarse estimation algorithm to further reduce the complexity:** A coarse estimation algorithm based on spatial multiple signal classification (SMUSIC) [16] and subspace constrained VBI (SCVBI) [17] is proposed to narrow down the search range and significantly reduce the effective dimension of the ultra-high-dimensional sparse signal, further reducing the complexity of the overall algorithm.

The rest of the paper is organized as follows. In Section II, we present the system model. In Section III, we introduce the 3D location-domain sparse channel model and formulate the joint sensing and data recovery problem. The proposed EM-Turbo-BiSVBI algorithm for joint sensing and data recovery and SMUSIC-SCVBI algorithm for coarse estimation are presented in Section IV and V, respectively. Finally, simulation results and the conclusion are given in Section VI and VII, respectively.

Notation: Lowercase boldface letters denote vectors and uppercase boldface letters denote matrices. Let $(\cdot)^{-1}$, $(\cdot)^T$, $(\cdot)^H$, $\langle \cdot \rangle$, $\text{Diag}(\cdot)$, and $\text{BlockDiag}(\cdot)$ represent the inverse, transpose, conjugate transpose, expectation, diagonalization, and block diagonalization operations, respectively. \mathbf{I}_N is the $N \times N$ dimensional identity matrix. For a set Ω with its cardinal number $|\Omega|$, $\mathbf{x} \triangleq [x_n]_{n \in \Omega} \in \mathbb{C}^{|\Omega| \times 1}$ is a vector composed of elements indexed by Ω .

II. UPLINK SYSTEM MODEL IN MASSIVE MIMO-OFDM ISAC

A. System Architecture and Frame Structure

Consider the uplink of a massive MIMO-OFDM ISAC system, where one BS equipped with a uniform planar array (UPA) of $M = M_x \times M_z$ antennas serves K single-antenna

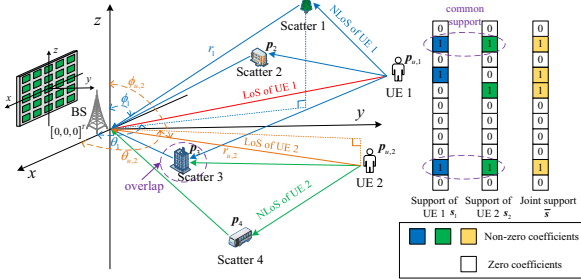


Figure 1: Illustration of the system model, the location-domain channels, and their non-zero coefficients.



Figure 2: Frame structure of the ISAC system.

users while sensing the scattering environment,¹ as illustrated in Fig. 1. In the spherical coordinate system, the BS's array is located at $\mathbf{p}_b = [0, 0, 0]^T$, and user k is located at $\mathbf{p}_{u,k} = [\theta_{u,k}, \phi_{u,k}, r_{u,k}]^T$, with $\theta_{u,k}$, $\phi_{u,k}$, and $r_{u,k}$ denoting the azimuth angle, elevation angle, and range of user k , respectively. Suppose there are a total number of L scatterers indexed by $l \in \mathcal{L} \triangleq \{1, \dots, L\}$ in the scattering environment, and the l -th scatterer is located at $\mathbf{p}_l = [\theta_l, \phi_l, r_l]^T$, $l \in \mathcal{L}$ in a 3-D area \mathcal{R} . Besides, we assume there are L_k scatterers contributing to the channel paths between user k and the BS, denoted by the index set $\mathcal{L}_k \subseteq \mathcal{L}$. Moreover, we assume the BS has some prior information about the users' location based on existing localization technologies, e.g., Global Positioning System (GPS) or the previous user localization result.²

The time is divided into frames, with each frame containing four phases: the uplink pilot and data transmission phases, the downlink pilot and data transmission phases, as illustrated in Fig. 2. We will focus on the uplink phase that combines the scattering environment sensing and data recovery into a single procedure. The pilot and data transmission phases contain T_p and T_d OFDM symbols indexed by $t_p \in \mathcal{T}_p \triangleq \{1, \dots, T_p\}$ and $t_d \in \mathcal{T}_d \triangleq \{1, \dots, T_d\}$, respectively, and each OFDM symbol contains N subcarriers indexed by $n \in \mathcal{N} \triangleq \{1, \dots, N\}$. In the t_p -th pilot symbol, each user k is allocated with a subset of pilot subcarriers denoted by $\mathcal{N}_{t_p,k}^p \subseteq \mathcal{N}$. In the t_d -th data symbol, each user k is allocated with a subset of data subcarriers denoted by $\mathcal{N}_{t_d,k}^d \subseteq \mathcal{N}$. The users are allocated with orthogonal pilot subcarriers to avoid interference. However, multiple users can share the same data subcarrier to achieve the spatial multiplexing gain.

¹For clarity, we focus on the case when each user has a single-antenna. However, the proposed algorithm can be readily extended to the case when each user has multiple antennas and transmits multiple data streams by treating each antenna/data stream as a virtual user with a single antenna/data stream.

²The knowledge of the transmitter location (i.e., the user location in this case) is usually required for performing scatterer localization [18], [19].

B. Uplink Signal Model for Joint Sensing and Data Recovery

The received uplink pilot signal on the n -th subcarrier of the t_p -th pilot symbol can be expressed as

$$\mathbf{y}_{t_p,n}^p = \mathbf{h}_{k_{t_p,n}^p, n} u_{t_p, k_{t_p,n}^p, n} + \mathbf{z}_{t_p,n}^p, \quad (1)$$

where $\mathbf{h}_{k_{t_p,n}^p, n} \in \mathbb{C}^{M \times 1}$ denotes the uplink channel vector of user $k_{t_p,n}^p$ on subcarrier n , $u_{t_p, k_{t_p,n}^p, n}$ denotes the pilot signal of user $k_{t_p,n}^p$, $\mathbf{z}_{t_p,n}^p \in \mathbb{C}^{M \times 1}$ is the additive white Gaussian noise (AWGN) with variance $1/\gamma$, and $k_{t_p,n}^p$ is the user allocated with the n -th pilot subcarrier in the t_p -th pilot symbol.

Similarly, the received uplink data signal on the n -th subcarrier of the t_d -th data symbol can be expressed as

$$\mathbf{y}_{t_d,n}^d = \sum_{k \in \mathcal{K}_{t_d,n}^d} \mathbf{h}_{k,n} x_{t_d,k,n} + \mathbf{z}_{t_d,n}^d, \quad (2)$$

where $x_{t_p,k,n} \sim \mathcal{CN}(x_{t_p,k,n}; 0, \sigma_{k,n}^2)$ denotes the data of user k with $\sigma_{k,n}^2$ denoting the transmit power of user k on subcarrier n , $\mathbf{z}_{t_d,n}^d \in \mathbb{C}^{M \times 1}$ is the AWGN with variance $1/\gamma$, and $\mathcal{K}_{t_d,n}^d$ is the set of users that are allocated with the n -th data subcarrier in the t_d -th data symbol.

The channel vector $\mathbf{h}_{k,n}$ can be modeled as $\mathbf{h}_{k,n} = \mathbf{h}_{k,n}^L + \mathbf{h}_{k,n}^{NL}$ with the line-of-sight (LoS) component $\mathbf{h}_{k,n}^L$ and non-LoS (NLoS) component $\mathbf{h}_{k,n}^{NL}$ given by

$$\mathbf{h}_{k,n}^L = \alpha_{k,0} e^{-j2\pi n f_0(\tau_{o,k} + \tau_0(\mathbf{p}_{u,k}))} \mathbf{a}(\theta_{u,k}, \phi_{u,k}), \quad (3a)$$

$$\mathbf{h}_{k,n}^{NL} = \sum_{l \in \mathcal{L}_k} \alpha_{k,l} e^{-j2\pi n f_0(\tau_{o,k} + \tau(\mathbf{p}_l, \mathbf{p}_{u,k}))} \mathbf{a}(\theta_l, \phi_l), \quad (3b)$$

where $\alpha_{k,0}$ is the complex gain of the LoS channel path, $\alpha_{k,l}$ is the complex gain of the l -th NLoS channel path, $\tau_{o,k}$ denotes the timing synchronization error between user k and the BS, $\tau_0(\mathbf{p}_{u,k}) = \frac{r_l}{c}$ is the propagation delay of the LoS path from user k to the BS with c denoting the speed of light,

$$\tau(\mathbf{p}_l, \mathbf{p}_{u,k}) = \frac{\sqrt{r_{u,k}^2 + r_l^2 - 2r_{u,k}r_l g(\mathbf{p}_l, \mathbf{p}_{u,k})}}{c} + \frac{r_l}{c}, \quad (4)$$

$$g(\mathbf{p}_l, \mathbf{p}_{u,k}) = \sin(\phi_{u,k}) \sin(\phi_l) \cos(\theta_{u,k} - \theta_l) + \cos(\phi_{u,k}) \cos(\phi_l), \quad (5)$$

is the propagation delay of the NLoS path from user k to the BS via the l -th scatterer, and $\mathbf{a}(\theta, \phi)$ is the array response vector for the UPA. Note that any multiple-bounce NLoS path of user k with arbitrary angles (θ, ϕ) and delay τ can be equivalent to a single-bounce NLoS path corresponding to a virtual scatterer at $\mathbf{p} = (\theta, \phi, r)$, where r is the solution of

$$\sqrt{r_{u,k}^2 + r^2 - 2r_{u,k}r g(\mathbf{p}, \mathbf{p}_{u,k})} + r - c\tau = 0. \quad (6)$$

In the uplink of the massive MIMO-OFDM ISAC system, both the received pilot and data signals $\mathbf{y}_{t_p,n}$ and $\mathbf{y}_{t_d,n}$ are exploited to sense the scattering environment, i.e., detect the number of active scatterers in $\mathcal{L}_k, \forall k$ associated with each user location $\mathbf{p}_k, \forall k$, and estimate the locations of all scatterers $\mathbf{p}_l, l \in \mathcal{L}$. In addition, the time offsets $\tau_{o,k}$'s and the user locations $\mathbf{p}_{u,k}$'s will also be estimated/refined to mitigate those imperfect factors. The sensing results can be

used to reconstruct the channel vectors for data recovery and the recovered data can be used to further enhance the sensing performance. As such, sensing and communications can enhance each other by performing a joint sensing and data recovery algorithm at the BS.

III. BILINEAR SPARSE BAYESIAN INFERENCE FORMULATION

In this section, we first obtain a location-domain sparse representation of the channel vectors. Then, we introduce a three-layer BGG prior to capture the joint sparsity of MU channels. Finally, we formulate joint sensing and data recovery as a bilinear sparse Bayesian inference problem.

A. 3D Location-Domain Sparse Representation

We introduce a grid-based method to obtain a sparse representation of the NLoS channel. Specifically, let

$$(\bar{\theta}, \bar{\phi}) = \{(\bar{\theta}_{i,j}, \bar{\phi}_{i,j}) \mid i = 1, \dots, Q_1, j = 1, \dots, Q_2\}, \quad (7)$$

denote $Q_a \triangleq Q_1 \times Q_2$ angle grid points and define $g_1(\theta, \phi) = \cos(\theta) \sin(\phi)$, $g_2(\phi) = \cos(\phi)$. Then, the angle grid points are chosen to satisfy

$$\begin{aligned} g_1(\bar{\theta}_{i,j}, \bar{\phi}_{i,j}) &= -\frac{Q_1 - 1}{Q_1} + \frac{2(i-1)}{Q_1}, \\ g_2(\bar{\phi}_{i,j}) &= -\frac{Q_2 - 1}{Q_2} + \frac{2(j-1)}{Q_2}, \end{aligned} \quad (8)$$

for $i = 1, \dots, Q_1$ and $j = 1, \dots, Q_2$. In other words, the angle grid is uniform in the transformed angular domain $g_1(\theta, \phi), g_2(\phi)$. Besides, the Q_r range grid points $\{\bar{r}_1, \bar{r}_2, \dots, \bar{r}_{Q_r}\}$ are uniformly placed in the range domain itself. Finally, the 3-D uniform position grid $\{\bar{r}_1, \dots, \bar{r}_Q\} \subset \mathcal{R}$ with $Q \triangleq Q_a \times Q_r \gg L$ positions is given by the $Q_a \times Q_r$ combinations between the Q_a angle grid points and Q_r range grid points.

In practice, the true positions of scatterers usually do not lie exactly on the grid. Therefore, it is essential to overcome the position mismatches for high-resolution localization. One common solution is to introduce a dynamic position grid, denoted by $\mathbf{r} \triangleq [\mathbf{r}_1; \dots; \mathbf{r}_Q]$ with $\mathbf{r}_q = [\theta_q, \phi_q, r_q]^T$, instead of only using a fixed position grid. In this case, there always exists a grid \mathbf{r}^* that covers the true positions of all scatterers. In general, the uniform grid is chosen as the initial point for \mathbf{r} in the algorithm, which makes it easier to find a good solution for the non-convex estimation problem [7].

Based on the dynamic position grid \mathbf{r} , we define a sparse basis $\mathbf{A}(\mathbf{r}) \in \mathbb{C}^{M \times Q}$ as

$$\mathbf{A}(\mathbf{r}) \triangleq [\mathbf{a}(\theta_1, \phi_1), \dots, \mathbf{a}(\theta_Q, \phi_Q)] \in \mathbb{C}^{M \times Q}. \quad (9)$$

Then, the sparse representation of the NLoS channel vector on the n -th subcarrier is given by

$$\mathbf{h}_{k,n}^{\text{NL}} = \mathbf{A}(\mathbf{r}) \mathbf{D}_{k,n}(\mathbf{r}) \boldsymbol{\alpha}_k, \quad (10)$$

where $\mathbf{D}_{k,n}(\mathbf{r})$ is a diagonal matrix with the q -th diagonal elements being $e^{-j2\pi n f_0(\tau_{o,k} + \tau(\mathbf{r}_q, \mathbf{p}_{u,k}))}$, $\boldsymbol{\alpha}_k \in \mathbb{C}^{Q \times 1}$ is called the location-domain NLoS sparse channel vector. $\boldsymbol{\alpha}_k$ only has

a few non-zero elements corresponding to the positions of scatterers in \mathcal{L}_k . Specifically, the q -th element of $\boldsymbol{\alpha}_k$, denoted by $\alpha_{k,q}$, represents the complex channel gain of the channel path with the corresponding scatterer lying in the position \mathbf{r}_q .

B. Three-layer BGG Prior Model

In practice, the MU channels exhibit certain joint sparsity as explained in Section II, i.e., the sets \mathcal{L}_k 's have intersections. In this subsection, we shall introduce a three-layer BGG prior model to capture the joint sparsity of the location-domain MU channels. Specifically, let $\boldsymbol{\rho}_k \triangleq [\rho_{k,1}, \dots, \rho_{k,Q}]^T$ represent the precision vector of $\boldsymbol{\alpha}_k$, where $1/\rho_{k,q}$ is the variance of $\alpha_{k,q}$. Let $\mathbf{s}_k \triangleq [s_{k,1}, \dots, s_{k,Q}]^T \in \{0, 1\}^Q$ represent the support vector of $\boldsymbol{\alpha}_k$. If there is a scatterer of user k around the q -th position grid \mathbf{r}_q , we have $s_{k,q} = 1$ and $\alpha_{k,q}$ is non-zero. Otherwise, we have $s_{k,q} = 0$ and $\alpha_{k,q} = 0$. Then, we introduce a joint support vector $\bar{\mathbf{s}} \triangleq [\bar{s}_1, \dots, \bar{s}_Q]^T \in \{0, 1\}^Q$ to represent the union of the positions of all scatterers in \mathcal{L} , i.e.,

$$\bar{s}_q = s_{1,q} \vee s_{2,q} \vee \dots \vee s_{K,q},$$

where \vee is the binary logical OR operator. In the proposed three-layer model, the joint distribution of $\{\boldsymbol{\alpha}_k, \boldsymbol{\rho}_k, \mathbf{s}_k, \bar{\mathbf{s}} \mid \forall k\}$ is represented as

$$\begin{aligned} & p(\{\boldsymbol{\alpha}_k, \boldsymbol{\rho}_k, \mathbf{s}_k, \bar{\mathbf{s}}\}) \\ &= p(\bar{\mathbf{s}}) \underbrace{\prod_{k=1}^K p(\mathbf{s}_k \mid \bar{\mathbf{s}})}_{\text{Support}} \underbrace{p(\boldsymbol{\rho}_k \mid \mathbf{s}_k)}_{\text{Precision}} \underbrace{p(\boldsymbol{\alpha}_k \mid \boldsymbol{\rho}_k)}_{\text{Sparse signal}}. \end{aligned}$$

A similar three-layer model has been considered in [18], [20] and is shown to be more flexible to capture the structured sparsity of realistic channels.

Conditioned on $\boldsymbol{\rho}_k$, the sparse channel $\boldsymbol{\alpha}_k$ is assumed to have independent complex Gaussian distributions with zero mean and variance $1/\rho_{k,q}$, i.e.,

$$p(\boldsymbol{\alpha}_k \mid \boldsymbol{\rho}_k) = \prod_q \mathcal{CN}\left(\alpha_{k,q}; 0, \frac{1}{\rho_{k,q}}\right). \quad (11)$$

The conditional distribution $p(\boldsymbol{\rho}_k \mid \mathbf{s}_k)$ is given by

$$\begin{aligned} p(\boldsymbol{\rho}_k \mid \mathbf{s}_k) &= \prod_q (\delta(s_{k,q} - 1) \Gamma(\rho_{k,q}; a, b) \\ &\quad + \delta(s_{k,q}) \Gamma(\rho_{k,q}; \bar{a}, \bar{b})), \end{aligned} \quad (12)$$

where $\delta(\cdot)$ is the Dirac Delta function, $\Gamma(\rho; a, b)$ is a Gamma hyper-prior with shape parameter a and rate parameter b . When $s_{k,q} = 1$, $\alpha_{k,q}$ is a non-zero element and the corresponding variance $1/\rho_{k,q}$ is $\Theta(1)$. In this case, a and b should be chosen to satisfy $\frac{a}{b} = \mathbb{E}(\rho_{k,q}) = \Theta(1)$. When $s_{k,q} = 0$, $\alpha_{k,q}$ is a zero element and the corresponding variance $1/\rho_{k,q}$ is close to zero. In this case, \bar{a} and \bar{b} should be chosen to satisfy $\frac{\bar{a}}{\bar{b}} = \mathbb{E}(\rho_{k,q}) \gg 1$. A typical value is $a = 1$, $b = 1$, $\bar{a} = 1$, and $\bar{b} = 10^{-5}$ [20].

The conditional probability for the support vector is given

by $p(s_k | \bar{s}) = \prod_q p(s_{k,q} | \bar{s}_q)$ with

$$p(s_{k,q} | \bar{s}_q) = \delta(\bar{s}_q) \delta(s_{k,q}) + \delta(\bar{s}_q - 1) \times (\delta(s_{k,q} - 1) \lambda_{k,q} + \delta(s_{k,q}) (1 - \lambda_{k,q})), \quad (13)$$

where $\lambda_{k,q}$ represents the probability of $s_{k,q} = 1$ conditioned on $\bar{s}_q = 1$, depicting the degree of overlap between scatterers of individual users and global scatterers. The joint support vector \bar{s} is modeled as an independent prior: $p(\bar{s}) = \prod_q p(\bar{s}_q)$ with $p(\bar{s}_q = 1) = \lambda_q$.

To automatically learn the noise precision, we assume a gamma distribution with shape parameter c and rate parameter d as the prior for γ , i.e., $p(\gamma) = \Gamma(\gamma; c, d)$. Let $\rho_{k,0}$ and $s_{k,0}$ denote the precision and support of the LoS channel gain $\alpha_{k,0}$, respectively. Then, the sparse prior model for the LoS channel $p(\alpha_{k,0}, \rho_{k,0}, s_{k,0})$ is similar except that there is no joint support, and the probability of $s_{k,0} = 1$ is $\lambda_{k,0}$.

C. Bilinear Sparse Bayesian Inference with Uncertain Parameters

For convenience, define pilot matrix $\mathbf{U}_{t_p} = [\mathbf{U}_{t_p,1}, \dots, \mathbf{U}_{t_p,K}]$ and data matrix $\mathbf{X}_{t_d} = [\mathbf{X}_{t_d,1}, \dots, \mathbf{X}_{t_d,K}]$ with

$$\mathbf{U}_{t_p,k} = \text{BlockDiag}(u_{t_p,k,1} \mathbf{I}_M, \dots, u_{t_p,k,N} \mathbf{I}_M), \\ \mathbf{X}_{t_d,k} = \text{BlockDiag}(x_{t_d,k,1} \mathbf{I}_M, \dots, x_{t_d,k,N} \mathbf{I}_M),$$

where $u_{t_p,k,n} = 0, \forall n \notin \mathcal{N}_{t_p,k}^p$ and $x_{t_d,k,n} = 0, \forall n \notin \mathcal{N}_{t_d,k}^d$. Let $\xi \triangleq \{r, p_u, \tau_o\}$ with $p_u = \{p_{u,1}, \dots, p_{u,k}\}$ denote the collection of sensing parameters. Moreover, define sensing matrix $\Phi(\xi) \triangleq \text{BlockDiag}(\Phi_1(\xi), \dots, \Phi_K(\xi))$, where

$$\Phi_k(\xi) \triangleq [\Phi_{k,n}^0, \Phi_{k,n}^1]_{n \in \mathcal{N}} \in \mathbb{C}^{MN \times (Q+1)}, \quad (14)$$

with

$$\Phi_{k,n}^0 = \left[e^{-j2\pi n f_0(\tau_{o,k} + \tau_o(p_{u,k}))} \mathbf{a}(\theta_{u,k}, \phi_{u,k}) \right], \\ \Phi_{k,n}^1 = [\mathbf{A}(r) \mathbf{D}_{k,n}(r)].$$

Then, using the location-domain sparse representation in (10), the received pilot and data signals on all available subcarriers can be expressed as

$$\mathbf{y}_{t_p}^p = \mathbf{U}_{t_p} \Phi(\xi) \alpha + \mathbf{z}^p, \forall t_p, \quad (15a)$$

$$\mathbf{y}_{t_d}^d = \mathbf{X}_{t_d} \Phi(\xi) \alpha + \mathbf{z}^d, \forall t_d, \quad (15b)$$

respectively, where $\mathbf{y}_{t_p}^p \triangleq [\mathbf{y}_{t_p,n}^p]_{n \in \mathcal{N}} \in \mathbb{C}^{MN \times 1}$, $\mathbf{y}_{t_d}^d \triangleq [\mathbf{y}_{t_d,n}^d]_{n \in \mathcal{N}} \in \mathbb{C}^{MN \times 1}$, $\alpha = [\bar{\alpha}_1^T, \dots, \bar{\alpha}_K^T]^T$ with $\bar{\alpha}_k = [\alpha_{k,0}, \alpha_k^T]^T$, $\mathbf{z}_{t_p}^p \triangleq [\mathbf{z}_{t_p,n}^p]_{n \in \mathcal{N}} \in \mathbb{C}^{MN \times 1}$, and $\mathbf{z}_{t_d}^d \triangleq [\mathbf{z}_{t_d,n}^d]_{n \in \mathcal{N}} \in \mathbb{C}^{MN \times 1}$.

For given sensing parameters ξ and data $\mathbf{x}_{t_d} = [\mathbf{x}_{t_d,1}^T, \dots, \mathbf{x}_{t_d,N}^T]^T \in \mathbb{C}^{\sum_{n=1}^N |\mathcal{K}_{t_d,n}^d| \times 1}$ with $\mathbf{x}_{t_d,n} = [\mathbf{x}_{t_d,k,n}]_{k \in \mathcal{K}_{t_d,n}^d} \in \mathbb{C}^{|\mathcal{K}_{t_d,n}^d| \times 1}, \forall t_d, n$, (15a) and (15b) form a linear observation model for the estimation of channel α . For given channel α and sensing parameters ξ , (15b) also forms a linear observation model for data recovery as

$$\mathbf{y}_{t_d,n}^d = \Psi_n(\xi) \mathbf{x}_{t_d,n} + \mathbf{z}_{t_d,n}^d, \forall t_d, n.$$

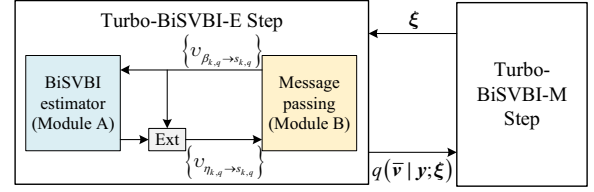


Figure 3: Framework of the EM-Turbo-BiSVBI algorithm.

where

$$\Psi_n(\xi) \triangleq \left[\left[(\Phi_{k,n}(\xi) \bar{\alpha}_k)^T \right]_{k \in \mathcal{K}_{t_d,n}^d} \right]^T \in \mathbb{C}^{M \times |\mathcal{K}_{t_d,n}^d|} \quad (16)$$

$$\text{with } \Phi_{k,n}(\xi) \triangleq [\Phi_{k,n}^0, \Phi_{k,n}^1] \in \mathbb{C}^{M \times (Q+1)}.$$

Therefore, (15a) and (15b) is a bilinear observation model w.r.t. α and \mathbf{x}_{t_d} 's with uncertain sensing parameters ξ .

To simplify the notation, the precision vector and the support vector of α are respectively defined as

$$\rho \triangleq [\rho_{1,0}, \rho_1^T, \dots, \rho_{K,0}, \rho_K^T]^T, \\ s \triangleq [s_{1,0}, s_1^T, \dots, s_{K,0}, s_K^T]^T.$$

Our primary goal is to estimate the channel vector α , the data vector $\mathbf{x} \triangleq [(\mathbf{x}_1)^T, \dots, (\mathbf{x}_{T_d})^T]^T$, the support vector s , and the uncertain parameters ξ given observation $\mathbf{y} \triangleq [(\mathbf{y}_1^p)^T, \dots, (\mathbf{y}_{T_p}^p)^T, (\mathbf{y}_1^d)^T, \dots, (\mathbf{y}_{T_d}^d)^T]^T$. To be specific, for given ξ , we aim at computing the conditional marginal posteriors, i.e., $p(\alpha | \mathbf{y}; \xi)$, $p(\mathbf{x} | \mathbf{y}; \xi)$, and $p(s_i | \mathbf{y}; \xi), \forall i$. On the other hand, the uncertain parameters ξ are obtained by the MAP estimator as follows:

$$\xi^* = \arg \max_{\xi} \ln p(\mathbf{y}, \xi) \\ = \arg \max_{\xi} \ln \int_{\bar{\mathbf{v}}} p(\mathbf{y}, \bar{\mathbf{v}}; \xi) p(\xi), \quad (17)$$

where $\bar{\mathbf{v}} \triangleq \{\alpha, \mathbf{x}, \rho, s, \bar{s}, \gamma\}$ denotes the collection of all variables, and $p(\xi)$ denotes the known prior distribution of ξ . Once we obtain the MAP estimate of ξ^* , we can obtain the minimum mean square error (MMSE) estimate of α as $\alpha^* = \int_{\alpha} \alpha p(\alpha | \mathbf{y}; \xi^*)$, and the MAP estimate of s as $s_{k,q}^* = \arg \max_{s_{k,q}} p(s_{k,q} | \mathbf{y}; \xi^*), \forall k, q$. Moreover, the marginal posteriors $p(\mathbf{x} | \mathbf{y}; \xi)$ for the data can be used as a soft information for digital demodulation and channel decoding.

However, it is exceedingly challenging to calculate the above conditional marginal posteriors precisely due to the looped factor graph. In the following section, we present the EM-Turbo-BiSVBI algorithm to solve this problem efficiently.

IV. EM-TURBO-BISVBI ALGORITHM

A. Outline of the EM-Turbo-BiSVBI Algorithm

As illustrated in Fig. 3, the EM-Turbo-BiSVBI algorithm iterates between the following two major steps until convergence.

- Turbo-BiSVBI-E Step:** For given $\xi^{(t)}$ in the t -th iteration, apply the turbo approach to combine the

Table I: Factors, Distributions, and Functional forms in Fig. 4.

Factor	Distribution	Functional form
$f_{t_p}^p$	$p(\mathbf{y}_{t_p}^p \boldsymbol{\alpha})$	$\mathcal{CN}(\mathbf{y}_{t_p}^p; \mathbf{U}_{t_p} \boldsymbol{\Phi}(\boldsymbol{\xi}) \boldsymbol{\alpha}, 1/\gamma)$
$f_{t_d}^d$	$p(\mathbf{y}_{t_d}^d \mathbf{x}_{t_d}, \boldsymbol{\alpha})$	$\mathcal{CN}(\mathbf{y}_{t_d}^d; \mathbf{X}_{t_d} \boldsymbol{\Phi}(\boldsymbol{\xi}) \boldsymbol{\alpha}, 1/\gamma)$
$g_{t_d}^d$	$\prod_{k,n} p(x_{t_d,k,n})$	$\prod_{k,n} \mathcal{CN}(x_{t_d,k,n}; 0, \sigma_{t_d,k,n}^2)$
$g_{k,q}$	$p(\alpha_{k,q} \rho_{k,q})$	$\mathcal{CN}(\alpha_{k,q}; 0, 1/\rho_{k,q})$
$\eta_{k,q}$	$p(\rho_{k,q} s_{k,q})$	$\begin{cases} \Gamma(\rho_{k,q}; a, b), & s_{k,q} = 1 \\ \Gamma(\rho_{k,q}; \bar{a}, \bar{b}), & s_{k,q} = 0 \end{cases}$
$\beta_{k,q}$	$p(s_{k,q} \bar{s}_q)$	$\begin{cases} p(s_{k,q} = 1) = \lambda_{k,q}, & \bar{s}_q = 1 \\ s_{k,q} = 0, & \bar{s}_q = 0 \end{cases}$
κ_q	$p(\bar{s}_q)$	$p(\bar{s}_q = 1) = \lambda_q$

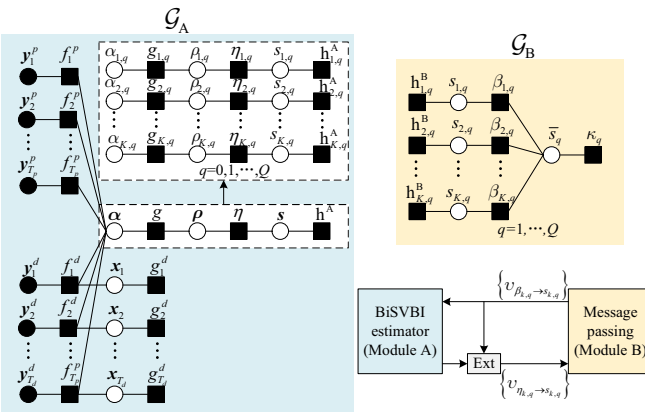


Figure 4: Module A and Module B of the Turbo-BiSVBI-E Step and messages flow between two modules.

BiSVBI method and the message passing method to calculate approximate marginal posteriors, denoted by $q(\bar{\mathbf{v}} | \mathbf{y}; \boldsymbol{\xi}^{(t)})$.

- **Turbo-BiSVBI-M Step:** Apply the EM method to construct a surrogate function for the MAP objective $\ln p(\mathbf{y}, \boldsymbol{\xi})$ based on $q(\bar{\mathbf{v}} | \mathbf{y}; \boldsymbol{\xi}^{(t)})$, then maximize the surrogate function with respect to $\boldsymbol{\xi}$.

In the following, we will elaborate the Turbo-BiSVBI-E and M Steps.

B. Turbo-BiSVBI-E Step

In the E step, the factor graph of the joint distribution $p(\mathbf{y}, \bar{\mathbf{v}}; \boldsymbol{\xi})$ is partitioned into two subgraphs, denoted by \mathcal{G}_A and \mathcal{G}_B , as shown in Fig. 4, where the expressions of each factor node are listed in Table I. To be more specific, \mathcal{G}_A describes the structure of the bilinear observation model with an independent BGG prior, while \mathcal{G}_B describes the more complicated sparse structure of the support vector $p(\mathbf{s}, \bar{\mathbf{s}})$ with effective binary observations. Correspondingly, two modules called Module A and B are designed to perform Bayesian inference over the two subgraphs.

Specifically, the extrinsic messages from Module A to B are $\{v_{\eta_{k,q} \rightarrow s_{k,q}}\}$, while the extrinsic messages from Module B to A are $\{v_{\beta_{k,q} \rightarrow s_{k,q}}\}$, as shown in Fig. 4. For convenience,

we define two turbo-iteration factor nodes to represent the extrinsic messages in \mathcal{G}_A and \mathcal{G}_B :

$$h_{k,q}^A \triangleq v_{\beta_{k,q} \rightarrow s_{k,q}}(s_{k,q}) \quad h_{k,q}^B \triangleq v_{\eta_{k,q} \rightarrow s_{k,q}}(s_{k,q}), \quad \forall k, q. \quad (18)$$

For each turbo iteration, Module A treats $h_{k,q}^A$ as the prior and performs the BiSVBI to calculate the approximate conditional posteriors $q(s_{k,q})$'s. Then, Module A passes extrinsic messages to Module B by subtracting the prior information from posterior information, i.e.,

$$h_{k,q}^B \triangleq v_{\eta_{k,q} \rightarrow s_{k,q}}(s_{k,q}) \propto q(s_{k,q}) / h_{k,q}^A. \quad (19)$$

Similarly, Module B treats $h_{k,q}^B$ as the binary observation information and performs message passing over \mathcal{G}_B and passes the extrinsic messages $h_{k,q}^A \triangleq v_{\beta_{k,q} \rightarrow s_{k,q}}(s_{k,q})$ to Module A. The two modules iterate until they reach a point of convergence.

Since Module B is a simply tree graph and the associated marginal posteriors can be easily calculated via sum-product message passing [21], we will only elaborate on Module A (BiSVBI) in the next subsection.

C. BiSVBI Module (Module A)

1) *Formulation of BiSVBI:* The BiSVBI module generalizes the SC-VBI in [17] from a linear observation model to a bilinear model to calculate the approximate marginal posteriors $q(\mathbf{v})$ for fixed sensing parameters $\boldsymbol{\xi}$, where $\mathbf{v} \triangleq \{\boldsymbol{\alpha}, \mathbf{x}, \boldsymbol{\rho}, \mathbf{s}, \gamma\}$. To be more specific, the turbo-iteration factor nodes $h_{k,q}^A(s_{k,q})$, $\forall k, q$ incorporate the prior information from Module B. Therefore, the following prior distribution is assumed in the BiSVBI module:

$$\begin{aligned} \hat{p}(\mathbf{v}) &= \hat{p}(\mathbf{s}) p(\boldsymbol{\rho} | \mathbf{s}) p(\boldsymbol{\alpha} | \boldsymbol{\rho}) p(\mathbf{x}) p(\gamma), \\ \hat{p}(\mathbf{s}) &= \prod_{k=1}^K \prod_{q=1}^Q h_{k,q}^A(s_{k,q}). \end{aligned} \quad (20)$$

Since the sensing parameter $\boldsymbol{\xi}$ is fixed in BiSVBI, we omit $\boldsymbol{\xi}$ in all notations in this subsection.

For convenience, we use $\mathbf{v}^k, k \in \mathcal{H} \triangleq \{1, 2, \dots, 5\}$ to denote an individual variable in \mathbf{v} . Denote $\hat{p}(\mathbf{v} | \mathbf{y})$ as the posterior distribution of \mathbf{v} with the prior $\hat{p}(\mathbf{v})$ in (20). Based on the VBI method, the approximate marginal posterior could be calculated by minimizing the KLD between $\hat{p}(\mathbf{v} | \mathbf{y})$ and $q(\mathbf{v})$, subject to a factorized form constraint as [22]

$$\mathcal{A}_{\text{VBI}}: \quad q^*(\mathbf{v}) = \arg \min_{q(\mathbf{v})} \int q(\mathbf{v}) \ln \frac{q(\mathbf{v})}{\hat{p}(\mathbf{v} | \mathbf{y})} d\mathbf{v}, \quad (21)$$

$$\text{s.t.} \quad q(\mathbf{v}) = \prod_{k \in \mathcal{H}} q(\mathbf{v}^k), \quad \int q(\mathbf{v}^k) d\mathbf{v}^k = 1, \quad (22)$$

$$q(\boldsymbol{\alpha}) = \mathcal{CN}(\boldsymbol{\alpha}; \boldsymbol{\mu}_{\boldsymbol{\alpha}}, \text{Diag}(\boldsymbol{\sigma}_{\boldsymbol{\alpha}}^2)), \quad (23)$$

$$q(\mathbf{x}) = \mathcal{CN}(\mathbf{x}; \boldsymbol{\mu}_{\mathbf{x}}, \text{Diag}(\boldsymbol{\sigma}_{\mathbf{x}}^2)). \quad (24)$$

Note that we add an additional constraint that $q(\boldsymbol{\alpha})/q(\mathbf{x})$ is a Gaussian distribution with mean $\boldsymbol{\mu}_{\boldsymbol{\alpha}}/\boldsymbol{\mu}_{\mathbf{x}}$ and diagonal covariance matrix $\text{Diag}(\boldsymbol{\sigma}_{\boldsymbol{\alpha}}^2)/\text{Diag}(\boldsymbol{\sigma}_{\mathbf{x}}^2)$, where both the mean $\boldsymbol{\mu}_{\boldsymbol{\alpha}}/\boldsymbol{\mu}_{\mathbf{x}}$ and variance vector $\boldsymbol{\sigma}_{\boldsymbol{\alpha}}^2/\boldsymbol{\sigma}_{\mathbf{x}}^2$ are optimization variables. This additional constraint is imposed to avoid the high-dimensional matrix inverse for calculating the posterior

covariance matrix. And the high-dimensional matrix inverse for calculating the posterior mean will be avoided using the subspace constrained method. Since Problem \mathcal{AVBI} is non-convex, we aim at finding a stationary solution of \mathcal{AVBI} , denoted by $q^*(\mathbf{v})$, as defined below.

Definition 1 (Stationary Solution). $q^*(\mathbf{v}) = \prod_{k \in \mathcal{H}} q^*(\mathbf{v}^k)$ is called a stationary solution of Problem \mathcal{AVBI} if it satisfies all the constraints in \mathcal{AVBI} and $\forall k \in \mathcal{H}$,

$$q^*(\mathbf{v}^k) = \arg \min_{q(\mathbf{v}^k)} \int \prod_{l \neq k} q^*(\mathbf{v}^l) q(\mathbf{v}^k) \ln \frac{\prod_{l \neq k} q^*(\mathbf{v}^l) q(\mathbf{v}^k)}{\hat{p}(\mathbf{v} | \mathbf{y})}.$$

In particular, for $q(\boldsymbol{\alpha})$ and $q(\mathbf{x})$, the above minimization is over the optimization variables $\boldsymbol{\mu}_\alpha, \boldsymbol{\sigma}_\alpha^2$ and $\boldsymbol{\mu}_x, \boldsymbol{\sigma}_x^2$.

In the following, we shall derive the BiSVBI algorithm to find a stationary solution for \mathcal{AVBI} .

2) *Derivation of the BiSVBI Algorithm for \mathcal{AVBI} :* The BiSVBI algorithm finds a stationary solution of \mathcal{AVBI} via alternately optimizing each individual density $q(\mathbf{v}^k), k \in \mathcal{H}$. Specifically, for given $q(\mathbf{v}^l), \forall l \neq k$ and $\mathbf{v}^k \neq \boldsymbol{\alpha}$ or \mathbf{x} , the optimal $q(\mathbf{v}^k)$ that minimizes the KLD in \mathcal{AVBI} is given by [22]

$$q(\mathbf{v}^k) \propto \exp \left(\langle \ln \hat{p}(\mathbf{v}, \mathbf{y}) \rangle_{\prod_{l \neq k} q(\mathbf{v}^l)} \right), \quad (25)$$

where $\langle f(x) \rangle_{q(x)} = \int f(x) q(x) dx$ and $\hat{p}(\mathbf{v}, \mathbf{y})$ is the joint distribution with prior $\hat{p}(\mathbf{v})$. However, when $\mathbf{v}^k = \boldsymbol{\alpha}$ or \mathbf{x} , the optimal $q(\boldsymbol{\alpha})$ or $q(\mathbf{x})$ is no longer given by (25) due to the independence constraint, and it is characterized by the following lemma. Note that the expectation $\langle f(\mathbf{v}^k) \rangle_{q(\mathbf{v}^k)}$ w.r.t. its own approximate posterior will be simplified as $\langle f(\mathbf{v}^k) \rangle$.

Lemma 2. For given $q(\mathbf{v}^k), \mathbf{v}^k \neq \boldsymbol{\alpha}$, the optimal posterior mean $\boldsymbol{\mu}_\alpha$ and variance vector $\boldsymbol{\sigma}_\alpha^2$ that minimizes the KLD subject to $q(\boldsymbol{\alpha}) = \mathcal{CN}(\boldsymbol{\alpha}; \boldsymbol{\mu}_\alpha, \text{Diag}(\boldsymbol{\sigma}_\alpha^2))$ are given by

$$\boldsymbol{\mu}_\alpha = \arg \min_{\mathbf{u}_\alpha} \varphi_\alpha(\mathbf{u}_\alpha) \triangleq \mathbf{u}_\alpha^H \mathbf{W}_\alpha \mathbf{u}_\alpha - 2\Re \{ \mathbf{u}_\alpha^H \mathbf{b}_\alpha \},$$

$$\boldsymbol{\sigma}_\alpha^2 = \left[\mathbf{W}_{\alpha,1,0}^{-1}, \dots, \mathbf{W}_{\alpha,1,Q}^{-1}, \dots, \mathbf{W}_{\alpha,K,0}^{-1}, \dots, \mathbf{W}_{\alpha,K,Q}^{-1} \right]^T. \quad (26)$$

where $\mathbf{W}_\alpha = \text{Diag}(\langle \boldsymbol{\rho} \rangle) + \langle \kappa \rangle \langle \mathbf{A}_\alpha^H \mathbf{A}_\alpha \rangle$, $\mathbf{W}_{\alpha,k,q}$ is the $[(k-1)(Q+1) + q + 1]$ -th diagonal element of \mathbf{W}_α , and $\mathbf{b} = \langle \kappa \rangle \langle \mathbf{A}_\alpha^H \rangle \mathbf{y}$ with $\mathbf{A}_\alpha = [\mathbf{A}_\alpha^p; \mathbf{A}_\alpha^d]$,

$$\mathbf{A}_\alpha^p = [\mathbf{U}_1 \boldsymbol{\Phi}; \dots; \mathbf{U}_{T_p} \boldsymbol{\Phi}],$$

$$\mathbf{A}_\alpha^d = [\mathbf{X}_1 \boldsymbol{\Phi}; \dots; \mathbf{X}_{T_d} \boldsymbol{\Phi}].$$

Similarly, for given $q(\mathbf{v}^k), \mathbf{v}^k \neq \mathbf{x}$, the optimal posterior mean $\boldsymbol{\mu}_x$ and variance vector $\boldsymbol{\sigma}_x^2$ are given by

$$\boldsymbol{\mu}_{x,t_d,n} = \arg \min_{\mathbf{u}_{x,t_d,n}} \varphi_{x,t_d,n}(\mathbf{u}_{x,t_d,n})$$

$$\triangleq \mathbf{u}_{x,t_d,n}^H \mathbf{W}_{x,t_d,n} \mathbf{u}_{x,t_d,n} - 2\Re \{ \mathbf{u}_{x,t_d,n}^H \mathbf{b}_{x,t_d,n} \},$$

$$\boldsymbol{\sigma}_{x,t_d,n}^2 = \left[\mathbf{W}_{x,t_d,k,n}^{-1} \right]_{k \in \mathcal{K}_{t_d,n}^d}, \forall t_d, n. \quad (27)$$

where $\boldsymbol{\mu}_{x,t_d,n}$ and $\boldsymbol{\sigma}_{x,t_d,n}^2$ are the posterior mean and variance corresponding to $\mathbf{x}_{t_d,n}$, $\mathbf{W}_{x,t_d,n} \triangleq \text{Diag}(\boldsymbol{\sigma}_{x,t_d,n}^2) +$

$$\langle \kappa \rangle \langle \mathbf{Y}_n^H \mathbf{Y}_n \rangle \text{ with } \boldsymbol{\sigma}_{t_d,n}^2 = \left[\sigma_{k,n}^2 \right]_{k \in \mathcal{K}_{t_d,n}^d}, \mathbf{b}_{x,t_d,n} = \langle \kappa \rangle \langle \mathbf{Y}_n^H \rangle \mathbf{Y}_{t_d,n}^d, \text{ and } [\mathbf{W}_{x,t_d,k,n}]_{k \in \mathcal{K}_{t_d,n}^d} = \text{Diag}(\mathbf{W}_{x,t_d,n}).$$

Please refer to Appendix A for the detailed proof. Based on (25) and Lemma 2, the update equations of all variables are given below.

a) *Update Equation for $q(\boldsymbol{\alpha})$:* From Lemma 2, $q(\boldsymbol{\alpha})$ can be derived as

$$q(\boldsymbol{\alpha}) = \mathcal{CN}(\boldsymbol{\alpha}; \boldsymbol{\mu}_\alpha, \boldsymbol{\sigma}_\alpha^2), \quad (28)$$

where $\boldsymbol{\mu}_\alpha = \mathbf{W}_\alpha^{-1} \mathbf{b}_\alpha$ and $\boldsymbol{\sigma}_\alpha^2$ are given in (26). The update of the posterior mean $\boldsymbol{\mu}_\alpha = \mathbf{W}_\alpha^{-1} \mathbf{b}_\alpha$ involves a high-dimensional matrix inverse \mathbf{W}_α^{-1} , where $\mathbf{W}_\alpha \in \mathbb{C}^{K(Q+1) \times K(Q+1)}$. In the following, we propose a subspace constrained matrix inverse method together with a robust design to greatly reduce the complexity for updating $\boldsymbol{\mu}_\alpha$.

Let $\hat{\mathcal{S}}$ denote the estimated support of $\boldsymbol{\alpha}$ obtained in the previous iteration, as will be detailed soon. Define a vector $\boldsymbol{\mu}_\alpha^s$ such that

$$\boldsymbol{\mu}_\alpha^s = \langle \kappa \rangle \mathbf{W}_{\alpha,\hat{\mathcal{S}}}^{-1} \langle \mathbf{A}_{\alpha,\hat{\mathcal{S}}}^H \rangle \mathbf{y}, \quad (29)$$

and $\boldsymbol{\mu}_{\alpha,\hat{\mathcal{S}}^c}^s = \mathbf{0}$, where $\boldsymbol{\mu}_{\alpha,\hat{\mathcal{S}}}^s \in \mathbb{C}^{|\hat{\mathcal{S}}| \times 1}$, $\mathbf{W}_{\alpha,\hat{\mathcal{S}}} \in \mathbb{C}^{|\hat{\mathcal{S}}| \times |\hat{\mathcal{S}}|}$, and $\mathbf{A}_{\alpha,\hat{\mathcal{S}}} \in \mathbb{C}^{MN(T_p+T_d) \times |\hat{\mathcal{S}}|}$ are subvector/submatrices of $\boldsymbol{\mu}_\alpha^s$, \mathbf{W}_α , and \mathbf{A}_α with the element/column/row indices lying in $\hat{\mathcal{S}}$, and $\boldsymbol{\mu}_{\alpha,\hat{\mathcal{S}}^c}^s$ contains the rest elements of $\boldsymbol{\mu}_\alpha^s$. If $\hat{\mathcal{S}} = \mathcal{S}$, $\boldsymbol{\mu}_\alpha^s$ is expected to provide a good initial solution for minimizing $\varphi_\alpha(\mathbf{u}_\alpha)$ in (26) based on the gradient method.

To improve the robustness of the algorithm against the support estimation error, we choose the best initial point $\boldsymbol{\mu}_\alpha^0$ from the following two choices: 1) $\boldsymbol{\mu}_\alpha^s$ obtained by the subspace constrained matrix inverse as in (29); 2) the posterior mean $\boldsymbol{\mu}_\alpha^p$ from the previous iteration, depending on which choice gives a lower value of the objective function $\varphi(\boldsymbol{\mu}_\alpha^0)$. In the first few iterations, $\boldsymbol{\mu}_\alpha^s$ is expected to be a good choice because the subspace constrained matrix inverse can be used to accelerate the initial convergence speed, compared to the MM-based methods in [9], [23], [24] which completely avoid any matrix inverse. As the iterations go on, the posterior mean $\boldsymbol{\mu}_\alpha^p$ from the previous iteration becomes more and more accurate and it may also become a good initial point.

Then we apply the gradient update for $B_\alpha \geq 1$ times. Specifically, in the i -th gradient iteration, the posterior mean is updated as

$$\boldsymbol{\mu}_\alpha^{(i)} = \boldsymbol{\mu}_\alpha^{(i-1)} - \epsilon_\alpha^{(i)} \nabla_{\mathbf{u}} \varphi(\mathbf{u}) |_{\mathbf{u}=\boldsymbol{\mu}_\alpha^{(i-1)}}, \quad (30)$$

where $\epsilon_\alpha^{(i)}$ is the step size determined by the Armijo rule,

$$\nabla_{\mathbf{u}} \varphi(\mathbf{u} = \boldsymbol{\mu}_\alpha^{(i-1)}) = \mathbf{W}_\alpha \boldsymbol{\mu}_\alpha^{(i-1)} - \mathbf{b}_\alpha, \quad (31)$$

and B_α is chosen to achieve a good trade-off between the per iteration complexity and convergence speed. Such a robust design ensures that the objective value $\varphi_\alpha(\mathbf{u}_\alpha)$ is decreased monotonically in each iteration until convergence to a stationary solution, as proved in Theorem 3.

Once we obtain the estimated posterior mean $\boldsymbol{\mu}_\alpha$, we can obtain an estimated support $\hat{\mathcal{S}}$ for the next iteration by finding

the elements in μ_α with sufficiently large energy. Specifically, we set a small threshold $\varepsilon > 0$ and compare each element of μ with the threshold to obtain the estimated support as

$$\hat{\mathcal{S}} \triangleq \left\{ k, q \mid \forall |\mu_{\alpha,k,q}|^2 > \varepsilon \right\}, \quad (32)$$

where the threshold ε is chosen according to the noise power $1/\langle \kappa \rangle$. A good choice for ε is 2 to 3 times the noise power $1/\langle \kappa \rangle$.

In the first iteration, we can simplify set $\hat{\mathcal{S}}$ according to the available prior information in practice or a simple baseline algorithm (e.g., using orthogonal matching pursuit (OMP) [25]). In Section V, we will propose a coarse estimation algorithm to further reduce the number of required grid points Q . In this case, $\hat{\mathcal{S}}$ in the first iteration can be obtained according to the coarse estimation result.

b) *Update Equation for $q(\rho)$:* $q(\rho)$ can be derived as

$$q(\rho) = \prod_{k=1}^K \prod_{q=1}^Q \Gamma(\rho_{k,q}; \check{a}_{k,q}, \check{b}_{k,q}), \quad (33)$$

where the approximate posterior parameters are given by:

$$\begin{aligned} \check{a}_{k,q} &= \langle s_{k,q} \rangle a_{k,q} + \langle 1 - s_{k,q} \rangle \bar{a}_{k,q} + 1, \\ \check{b}_{k,q} &= \langle s_{k,q} \rangle b_{k,q} + \langle 1 - s_{k,q} \rangle \bar{b}_{k,q} + \langle |\alpha_{k,q}|^2 \rangle. \end{aligned} \quad (34)$$

c) *Update Equation for $q(s)$:* $q(s)$ can be derived as

$$q(s) = \prod_{k=1}^K \prod_{q=1}^Q (\check{\lambda}_{k,q})^{s_{k,q}} (1 - \check{\lambda}_{k,q})^{1-s_{k,q}}, \quad (35)$$

where $\check{\lambda}_{k,q}$ is given by

$$\check{\lambda}_{k,q} = \frac{\lambda_{k,q} C_{k,q}}{\lambda_{k,q} C_{k,q} + (1 - \lambda_{k,q}) \bar{C}_{k,q}}, \quad (36)$$

with $\lambda_{k,q} = h_{k,q}^\alpha (s_{k,q} = 1)$, $C_{k,q} = \frac{b_{k,q}^{a_{k,q}}}{\Gamma(a_{k,q})} \exp((a_{k,q} - 1) \langle \ln \rho_{k,q} \rangle - b_n \langle \rho_{k,q} \rangle)$, and $\bar{C}_{k,q} = \frac{\bar{b}_{k,q}^{\bar{a}_{k,q}}}{\Gamma(\bar{a}_{k,q})} \exp((\bar{a}_{k,q} - 1) \langle \ln \rho_{k,q} \rangle - \bar{b}_{k,q} \langle \rho_{k,q} \rangle)$.

Here, $\Gamma(\cdot)$ denotes the gamma function.

d) *Update Equation for $q(x)$:* From Lemma 2, $q(x) = \prod_{t_d=1}^{T_d} \prod_{n=1}^N q(x_{t_d,n})$ with

$$q(x_{t_d,n}) = \mathcal{CN}(x_{t_d,n}; \mu_{x,t_d,n}, \sigma_{x,t_d,n}^2), \quad (37)$$

where $\mu_{x,t_d,n} = \mathbf{W}_{x,t_d,n}^{-1} \mathbf{b}_{x,t_d,n}$ and $\sigma_{x,t_d,n}^2$ are given in (27).

e) *Update Equation for $q(\kappa)$:* The posterior distribution $q(\kappa)$ is given by

$$q(\kappa) = \Gamma(\kappa; \check{c}, \check{d}), \quad (38)$$

where the parameters \check{c} and \check{d} are given by

$$\begin{aligned} \check{c} &= c + (T_p + T_d) MN, \\ \check{d} &= d + \left\langle \|\mathbf{y} - \mathbf{A}_\alpha \boldsymbol{\alpha}\|^2 \right\rangle_{q(\boldsymbol{\alpha})q(x)}. \end{aligned} \quad (39)$$

The expectations used in the above update equations are

summarized as follows:

$$\begin{aligned} \langle \rho_{k,q} \rangle &= \frac{\check{a}_{k,q}}{\check{b}_{k,q}}, \quad \langle s_{k,q} \rangle = \check{\lambda}_{k,q}, \quad \langle \kappa \rangle = \frac{\check{c}}{\check{d}}, \\ \langle \alpha_{k,q}^2 \rangle &= |\mu_{\alpha,k,q}|^2 + \sigma_{\alpha,k,q}^2, \quad \langle \ln \rho_{k,q} \rangle = \psi(\check{a}_{k,q}) - \ln \check{b}_{k,q}, \end{aligned}$$

where $\psi(\cdot) \triangleq d \ln(\Gamma(\cdot))$ denotes the logarithmic derivative of the gamma function. Note that the expectations $\langle \mathbf{A}_\alpha^H \mathbf{A}_\alpha \rangle$ and $\langle \mathbf{A}_\alpha \rangle$ are w.r.t. $q(\mathbf{x})$, and the expectations $\langle \boldsymbol{\Psi}_n^H \boldsymbol{\Psi}_n \rangle$ and $\langle \boldsymbol{\Psi}_n^H \rangle$ are w.r.t. $q(\boldsymbol{\alpha})$, and those expectations can be easily calculated and are omitted for conciseness.

3) *Convergence Analysis:* Despite the above approximations in the calculation of the posterior mean $\mu_\alpha = \mathbf{W}_\alpha^{-1} \mathbf{b}_\alpha$, we can show that the proposed BiSVBI still converges to a stationary point of \mathcal{A}_{VBI} , as stated in the following theorem, whose proof can be found in Appendix B.

Theorem 3 (Convergence of BiSVBI). *The BiSVBI algorithm monotonically decrease the KLD objective in \mathcal{A}_{VBI} , and every limiting point $q^*(\mathbf{v}) = \prod_{k \in \mathcal{H}} q^*(\mathbf{v}^k)$ generated by the BiSVBI is a stationary solution of Problem \mathcal{A}_{VBI} .*

D. Turbo-BiSVBI-M Step

Since there is no closed-form expression of $\ln p(\mathbf{y}, \boldsymbol{\xi})$, it is challenging to directly solve the maximization problem in (17). To get around this problem, one common solution is to construct a surrogate function of $\ln p(\mathbf{y}, \boldsymbol{\xi})$ and maximize the surrogate function with respect to $\boldsymbol{\xi}$. Specifically, in the t -th iteration, the surrogate function inspired by the EM method is given by

$$\begin{aligned} Q(\boldsymbol{\xi}; \boldsymbol{\xi}^{(t)}) &= \int_{\mathbf{v}} q^{(t)}(\bar{\mathbf{v}}) \ln \frac{p(\mathbf{y}, \bar{\mathbf{v}}; \boldsymbol{\xi})}{q^{(t)}(\bar{\mathbf{v}})} + \ln p(\boldsymbol{\xi}) \\ &= - \sum_{t_p=1}^{T_p} \langle \kappa \rangle \left\| \mathbf{y}_{t_p}^p - \mathbf{U}_{t_p} \boldsymbol{\Phi}(\boldsymbol{\xi}) \boldsymbol{\mu}_\alpha^{(t)} \right\|^2 \\ &\quad - \sum_{t_d=1}^{T_d} \langle \kappa \rangle \left\| \mathbf{y}_{t_d}^d - \langle \mathbf{X}_{t_d} \rangle \boldsymbol{\Phi}(\boldsymbol{\xi}) \boldsymbol{\mu}_\alpha^{(t)} \right\|^2 \\ &\quad + \ln p(\boldsymbol{\xi}) + C_2(\boldsymbol{\xi}) + C_0, \end{aligned} \quad (40)$$

where $q^{(t)}(\bar{\mathbf{v}}) \triangleq q(\bar{\mathbf{v}} | \mathbf{y}; \boldsymbol{\xi}^{(t)})$, $q^{(t)}(\boldsymbol{\alpha}) = \mathcal{CN}(\boldsymbol{\alpha}; \boldsymbol{\mu}_\alpha^{(t)}, (\boldsymbol{\sigma}_\alpha^{(t)})^2)$, and $q^{(t)}(\mathbf{x}_{t_d,n}) = \mathcal{CN}(\mathbf{x}_{t_d,n}; \boldsymbol{\mu}_{x,t_d,n}^{(t)}, (\boldsymbol{\sigma}_{x,t_d,n}^{(t)})^2)$ are the approximate posteriors calculated in the latest E-step, $\langle \mathbf{X}_{t_d} \rangle$ is obtained by replacing all $x_{t_d,k,n}$'s in \mathbf{X}_{t_d} with its posterior mean $\boldsymbol{\mu}_{t_d,k,n}^{(t)}$'s, $C_2(\boldsymbol{\xi})$ is related to the posterior variance $(\boldsymbol{\sigma}_\alpha^{(t)})^2$ and $(\boldsymbol{\sigma}_{x,t_d,n}^{(t)})^2$, and C_0 is a constant.

When $q^{(t)}(\bar{\mathbf{v}}) = p(\bar{\mathbf{v}} | \mathbf{y}; \boldsymbol{\xi}^{(t)})$, it can be shown that the gradient of $Q(\boldsymbol{\xi}; \boldsymbol{\xi}^{(t)})$ is consistent with $\ln p(\mathbf{y}, \boldsymbol{\xi})$ [20], and thus we can apply the gradient ascent method to update $\boldsymbol{\xi}$ as

$$\boldsymbol{\xi}^{(t+1)} = \boldsymbol{\xi}^{(t)} + \varepsilon^{(t)} \frac{\partial Q(\boldsymbol{\xi}; \boldsymbol{\xi}^{(t)})}{\partial \boldsymbol{\xi}}, \quad (41)$$

Algorithm 1 EM-Turbo-BiSVBI algorithm

Input: y , initial parameters $\xi^{(1)}$, inner iteration numbers I , outer iteration number T .

Output: $\hat{\alpha}$, \hat{x} , and $\hat{\xi}$.

- 1: **for** $t = 1, \dots, T$ **do**
- 2: **Turbo-BiSVBI-E Step:**
- 3: **% Module A: BiSVBI**
- 4: **for** $i = 1, \dots, I$ **do**
- 5: Update $q^{(t)}(\alpha)$ in (28), where the posterior mean μ_α is obtained by performing the gradient update (30) for B_x times with the initial point in (29).
- 6: Update $q^{(t)}(\rho)$ using (33).
- 7: Update $q^{(t)}(s)$ using (35).
- 8: Update $q^{(t)}(x)$ using (37).
- 9: Update $q^{(t)}(\kappa)$ using (38).
- 10: **end for**
- 11: Calculate the MMSE estimates $\alpha^{(t)}$, $x^{(t)}$, and $\kappa^{(t)}$, and then update the support set $\hat{\mathcal{S}}$ using (32).
- 12: Send the extrinsic messages $\{v_{\eta_{k,q} \rightarrow s_{k,q}}\}$ to Module B, using (19).
- 13: **% Module B: Message passing**
- 14: Perform message passing over \mathcal{G}_B and send the extrinsic messages $\{v_{\beta_{k,q} \rightarrow s_{k,q}}\}$ to Module A.
- 15: **Turbo-BiSVBI-M Step:**
- 16: Construct the surrogate function $Q(\xi; \xi^{(t)})$ in (40).
- 17: Update $\xi^{(t+1)}$ via gradient ascent, using (41).
- 18: **end for**
- 19: Output $\hat{\alpha} = \alpha^{(T)}$, $\hat{x} = x^{(T)}$, and $\hat{\xi} = \xi^{(T+1)}$.

where $\varepsilon^{(t)}$ is the step size determined by the Armijo rule. Such a gradient update method ensures that $\{\xi^{(t)}\}$ converges to a stationary solution of the MAP problem in (17) [20]. In practice, $q^{(t)}(\bar{v})$ is not exactly equal to the true posterior $p(\bar{v} | y; \xi^{(t)})$. Moreover, it is also a good practice to omit the variance term $\frac{\partial C_2(\xi)}{\partial \xi}$ in the gradient calculation to reduce the complexity. Since the variational posterior $q^{(t)}(\bar{v})$ obtained by the Turbo-BiSVBI algorithm is a good approximation for $p(\bar{v} | y; \xi^{(t)})$ and the variance term $C_2(\xi)$ is usually small, the more practical update in (41) based on the approximate gradient calculated using $q^{(t)}(\bar{v})$ and omitting $\frac{\partial C_2(\xi)}{\partial \xi}$ can still find a good solution of (17), as shown in the simulations.

The overall EM-Turbo-BiSVBI algorithm is summarized in Algorithm 1.

E. Complexity Analysis for Turbo-BiSVBI

The complexity of Turbo-BiSVBI is dominated by the update of $q(\alpha)$ and $q(x)$. In the update of $q(\alpha)$ in BiSVBI, the matrix inverse is constrained in the subspace of the estimated support, and thus the complexity order is only $\mathcal{O}(|\hat{\mathcal{S}}|^3)$. The complexity order of the matrix-vector multiplications in the gradient update (30) is $\mathcal{O}(K(Q+1)MN(T_p + T_d))$. In the update of $q(x)$ in BiSVBI, the complexity order of the matrix inverse and matrix multiplications to calculate the posterior mean $\mu_{x,t_d,n} = \mathbf{W}_{x,t_d,n}^{-1} \mathbf{b}_{x,t_d,n}$ is

$\mathcal{O}(M|\mathcal{K}_{t_d,n}^d|^2 + |\mathcal{K}_{t_d,n}^d|^3)$. Therefore, the overall complexity order per iteration of Turbo-BiSVBI is

$$\mathcal{O}\left(K(Q+1)MN(T_p + T_d) + |\hat{\mathcal{S}}|^3 + \sum_{t_d=1}^{T_d} \sum_{n=1}^N \left(M|\mathcal{K}_{t_d,n}^d|^2 + |\mathcal{K}_{t_d,n}^d|^3\right)\right). \quad (42)$$

In the original update of $q(\alpha)$ in BiSVBI, the high-dimensional matrix inverse $\mu_\alpha = \mathbf{W}_\alpha^{-1} \mathbf{b}_\alpha$ has a complexity order of $\mathcal{O}(K(Q+1))^3$, which is unacceptable in practice. The subspace constrained matrix inverse in BiSVBI significantly reduces the complexity order to only $\mathcal{O}(|\hat{\mathcal{S}}|^3)$, where $|\hat{\mathcal{S}}| \ll K(Q+1)$. In addition, the number of data streams per subcarrier $|\mathcal{K}_{t_d,n}^d| \leq K$ is usually small (e.g., typically less than 8 in current systems). Therefore, the complexity of the matrix inverse $\mathbf{W}_{x,t_d,n}^{-1}$ in the update of $q(x)$ is often acceptable since the dimension of $\mathbf{W}_{x,t_d,n}$ is only $|\mathcal{K}_{t_d,n}^d|$.

Remark 4 (Methods to further reduce the complexity). In practice, the K users are often divided into G groups such that only the users in the same group will be allocated with the same pilot/data subcarriers. In this case, $\mathbf{W}_{\alpha,\hat{\mathcal{S}}}^{-1}$, \mathbf{W}_α , and \mathbf{A}_α are all block diagonal matrices, and the complexity can be further reduced by exploiting the block diagonal structures. In addition, when the number of data streams $|\mathcal{K}_{t_d,n}^d|$ per subcarrier becomes large (say up to 100 streams in future systems), we can still avoid the matrix inverse in $\mu_{x,t_d,n} = \mathbf{W}_{x,t_d,n}^{-1} \mathbf{b}_{x,t_d,n}$ by first applying an inverse-free data recovery method [23], [24] to generate a good initial point $\mu_{x,t_d,n}^s$ and then apply the gradient updates for B_x times, similar to the gradient update for $\mu_\alpha^{(i)}$ in (30). With similar robust design as for $q(\alpha)$, the convergence of BiSVBI is still guaranteed. Finally, the number of grid points Q to cover the entire 3D area is usually huge, and thus the complexity order of the gradient update of $q(\alpha)$ is still high. In the following section, we propose an efficient coarse estimation algorithm to identify the angles of scatterers, which narrows down the search region and provides more prior information for the EM-Turbo-BiSVBI to significantly reduce the complexity and accelerate the convergence speed.

V. SMUSIC-SCVBI ALGORITHM FOR COARSE ESTIMATION

In this section, we propose a coarse estimation algorithm based on SMUSIC [16] and SCVBI [17] (called SMUSIC-SCVBI algorithm) to estimate the angles for each user. The SMUSIC-SCVBI algorithm first adopts SMUSIC to estimate the angles, and then refines the angles using SCVBI. In the following, we shall focus on presenting the SMUSIC-SCVBI algorithm for a reference user k . Note that in the coarse estimation stage, the data is not recovered, and only the pilot subcarriers can be used to estimate the delays. Since the number of pilot subcarriers is usually small in practice, we do not estimate the delays in the coarse estimation stage. However, if the number of pilot subcarriers is sufficient, it is also easy to incorporate the delay estimation into the coarse

estimation stage by replacing SMUSIC with spatial-temporary MUSIC (ST-MUSIC) [16].

A. SMUSIC to Estimate the Angles

In SMUSIC, the spatial-domain covariance matrix for user k is first calculated as

$$\begin{aligned} \mathbf{R}^s &= \frac{1}{N_s} \sum_{t_p=1}^{T_p} \sum_{n \in \mathcal{N}_{t_p,k}^p} \mathbf{y}_{t_p,n}^p \left(\mathbf{y}_{t_p,n}^p \right)^H \\ &+ \frac{1}{N_s} \sum_{t_d=1}^{T_d} \sum_{n \in \mathcal{N}_{t_d,k}^d} \mathbf{y}_{t_d,n}^d \left(\mathbf{y}_{t_d,n}^d \right)^H \\ &= \mathbf{V}_s^s \mathbf{\Lambda}_s^s \left(\mathbf{V}_s^s \right)^H + \mathbf{V}_n^s \mathbf{\Lambda}_n^s \left(\mathbf{V}_n^s \right)^H, \end{aligned} \quad (43)$$

where $N_s = \sum_{t_p=1}^{T_p} \left| \mathcal{N}_{t_p,k}^p \right| + \sum_{t_d=1}^{T_d} \left| \mathcal{N}_{t_d,k}^d \right|$ is the total number of available spatial samples, the column vectors of \mathbf{V}_s^s are the eigenvectors that span the signal subspace of \mathbf{R}^s , corresponding to the largest L_k eigenvalues. The number of multi-paths L_k can be estimated using the minimum descriptive length (MDL) criterion [26]. And the column vectors of \mathbf{V}_n^s are the eigenvectors that span the noise subspace of \mathbf{R}^s . $\mathbf{\Lambda}_s^s, \mathbf{\Lambda}_n^s$ are diagonal matrices consisting of the associated eigenvalues.

Then, the angles can be estimated at which the following pseudo-spectrum achieve maximum values [27]:

$$\mathcal{P}^s(\theta, \phi) = \frac{1}{\mathbf{a}(\theta, \phi)^H \mathbf{V}_n^s \left(\mathbf{V}_n^s \right)^H \mathbf{a}(\theta, \phi)}, \quad (44)$$

and let $(\tilde{\theta}_k, \tilde{\phi}_k) = \left[(\tilde{\theta}_{k,1}, \tilde{\phi}_{k,1}), \dots, (\tilde{\theta}_{k,\tilde{L}_k}, \tilde{\phi}_{k,\tilde{L}_k}) \right]^T$ denote the \tilde{L}_k angles found by the SMUSIC, i.e., \tilde{L}_k angles achieving the maximum values of $\mathcal{P}^s(\theta, \phi)$.

B. SCVBI to Refine the Angles

Let \mathcal{U}_k denote the set of users that share some data subcarriers with user k . Clearly, the received signals $\mathbf{y}_{t_d,n}^d$'s on the data subcarriers $n \in \mathcal{N}_{t_d,k}^d$ may also contain the data signals from the other users in \mathcal{U}_k . Therefore, the angles obtained by the SMUSIC may contain all angles of the users in \mathcal{U}_k . Since the pilot subcarriers in $\mathcal{N}_{t_p,k}^p$'s only contain pilot signals from user k , we can exploit the received pilot signals $\mathbf{y}_{t_p,n}^p$'s to identify the angles of user k and filter out the angles of the other users in \mathcal{U}_k .

Specifically, define the angular-domain sparse basis $\tilde{\mathbf{A}} \in \mathbb{C}^{M \times \tilde{L}_k}$ based on the estimated angles $(\tilde{\theta}_k, \tilde{\phi}_k)$ as

$$\tilde{\mathbf{A}} \triangleq \left[\mathbf{a} \left(\tilde{\theta}_{k,1}, \tilde{\phi}_{k,1} \right), \dots, \mathbf{a} \left(\tilde{\theta}_{k,\tilde{L}_k}, \tilde{\phi}_{k,\tilde{L}_k} \right) \right]. \quad (45)$$

Then the sparse representation of the angular-domain channel vector on the n -th subcarrier is given by

$$\mathbf{h}_{k,n} = \tilde{\mathbf{A}} \tilde{\boldsymbol{\alpha}}_{k,n}, \quad (46)$$

where $\tilde{\boldsymbol{\alpha}}_{k,n} = \left[\tilde{\alpha}_{k,n,1}, \dots, \tilde{\alpha}_{k,n,\tilde{L}_k} \right]^T$ is the angular-domain channel vector on subcarrier n . Then the received pilot signal can be rewritten as

$$\mathbf{y}_{t_p,n}^p = \tilde{\mathbf{A}} \tilde{\boldsymbol{\alpha}}_{k,n} + \mathbf{z}_{t_p,n}^p, \quad \forall t_p, \forall n \in \mathcal{N}_{t_p,k}^p. \quad (47)$$

Note that different $\tilde{\boldsymbol{\alpha}}_{k,n}$'s share a common support because the channels on different subcarriers share the same set of angles. As such, a similar three-layer BGG prior is introduced to capture such a common sparsity. In particular, a common support vector $\tilde{\mathbf{s}}_k \triangleq \left[\tilde{s}_{k,1}, \dots, \tilde{s}_{k,\tilde{L}_k} \right]^T \in \{0, 1\}^{\tilde{L}_k}$ is introduced to indicate the non-zero elements in $\tilde{\boldsymbol{\alpha}}_{k,n}$'s. Let $\tilde{\boldsymbol{\rho}}_{k,n} = \left[\tilde{\rho}_{k,n,1}, \dots, \tilde{\rho}_{k,n,\tilde{L}_k} \right]^T$ denote the precision vector of $\tilde{\boldsymbol{\alpha}}_{k,n}$. Then the joint distribution can be expressed as

$$p \left(\{\tilde{\boldsymbol{\alpha}}_{k,n}\}, \{\tilde{\boldsymbol{\rho}}_{k,n}\}, \tilde{\mathbf{s}}_k \right) \quad (48)$$

$$= p \left(\tilde{\mathbf{s}}_k \right) \prod_{n \in \mathcal{N}_k^p} p \left(\tilde{\boldsymbol{\rho}}_{k,n} \mid \tilde{\mathbf{s}}_k \right) p \left(\tilde{\boldsymbol{\alpha}}_{k,n} \mid \tilde{\boldsymbol{\rho}}_{k,n} \right), \quad (49)$$

where $\mathcal{N}_k^p = \cup_{t_p} \mathcal{N}_{t_p,k}^p$, $p \left(\tilde{\mathbf{s}}_k \right) = \prod_{l=1}^{\tilde{L}_k} \left(\tilde{\lambda}_{k,l} \right)^{\tilde{s}_{k,l}} \left(1 - \tilde{\lambda}_{k,l} \right)^{1-\tilde{s}_{k,l}}$, and $\tilde{\lambda}_{k,l}$ is the probability of $\tilde{s}_{k,l} = 1$, which is set to be $\tilde{\lambda}_{k,l} = \frac{1}{|\mathcal{U}_k|}$ in the simulations. $p \left(\tilde{\boldsymbol{\rho}}_{k,n} \mid \tilde{\mathbf{s}}_k \right)$ is a conditional Gamma distribution such that the mean value of $\tilde{\rho}_{k,n,l}$ is set to be $O(1)$ when $\tilde{s}_{k,l} = 1$ and a large value when $\tilde{s}_{k,l} = 0$. Finally, $p \left(\tilde{\boldsymbol{\alpha}}_{k,n,l} \mid \tilde{\boldsymbol{\rho}}_{k,n,l} \right) = \mathcal{CN} \left(\tilde{\alpha}_{k,n,l}; 0, \tilde{\rho}_{k,n,l}^{-1} \right), \forall l$.

With the linear observation model in (47) and the BGG sparse prior in (48), the problem of recovering $\tilde{\boldsymbol{\alpha}}_{k,n}$'s becomes a structured compressive sensing problem, which can be solved efficiently by the SCVBI algorithm [17]. SCVBI is a special case of BiSVBI and the details are omitted for conciseness. Once we obtain the estimated posterior mean $\tilde{\boldsymbol{\mu}}_{k,n}$ of $\tilde{\boldsymbol{\alpha}}_{k,n}$, we can obtain an estimated support $\tilde{\mathcal{S}}_{k,n}$ by finding the elements in $\boldsymbol{\mu}$ with sufficiently large energy. Then the angles of user k can be identified as $(\hat{\theta}_k, \hat{\phi}_k) = \left[(\hat{\theta}_{k,l}, \hat{\phi}_{k,l}) \right]_{l \in \tilde{\mathcal{S}}_{k,n}}^T$.

When the number of pilot subcarriers is small, the more precise angle information provided by the SMUSIC based on all subcarriers including the data subcarriers can significantly enhance the performance of angle detection and estimation in the SCVBI step. In practice, we can choose the total number of data subcarriers N_D used in the SMUSIC for all users to achieve a trade off between complexity and performance. When the number of pilot subcarriers is sufficient, we can even set $N_D = 0$, in which case the SMUSIC step is completely removed.

C. Compact Construction of the Position Grid

To reduce redundancy, we apply clustering to group similar angles in $(\hat{\theta}, \hat{\phi}) = \left\{ (\hat{\theta}_k, \hat{\phi}_k), k = 1, \dots, K \right\}$ and consolidate each angle cluster into a single representative angle grid point, thereby avoiding dense angle grids to reduce the complexity and also to avoid overfitting of the channel. Specifically, the clustering of angles is based on an oversampled uniform angle grid as defined in (7) and (8), with $Q_1 = N_o M_x$ and $Q_2 = N_o M_y$, where $N_o > 1$ can be chosen to achieve a trade off between the grid resolution and complexity, and a typical value of N_o is 2 or 4. The angles that fall within the same angle grid are considered to belong to the same cluster.

Specifically, let J denote the number of clusters, \mathcal{A}_j^c denote the set of angles in the j -th cluster, $(\theta_{j,i}^c, \phi_{j,i}^c), i \in \mathcal{A}_j^c$

denote the i -th angle in the j -th cluster and $\tilde{\alpha}_{j,i}^c$ denote the associated complex gain. Then the representative angle (θ_j^c, ϕ_j^c) for cluster j can be obtained as

$$(\theta_j^c, \phi_j^c) = \frac{\sum_{i \in \mathcal{A}_j^c} |\tilde{\alpha}_{j,i}^c|^2 (\theta_{j,i}^c, \phi_{j,i}^c)}{\sum_{i \in \mathcal{A}_j^c} |\tilde{\alpha}_{j,i}^c|^2}. \quad (50)$$

Finally, let \mathcal{C}_k denote the set of clusters that contains the angles of user k . Then the initial dynamic position grid for user k is given by the $Q_k = |\mathcal{C}_k| \times Q_r$ combinations between the $|\mathcal{C}_k|$ angle grid points $\{(\theta_j^c, \phi_j^c), j \in \mathcal{C}_k\}$ and Q_r uniform range grid points, and the union of the position grid of all users is given by the $Q = J \times Q_r$ combinations between the J angle grid points $\{(\theta_j^c, \phi_j^c), j = 1, \dots, J\}$ and Q_r uniform range grid points.

D. Complexity Analysis for the Overall Algorithm

The complexity of SMUSIC is upper bounded by [27]

$$\mathcal{O}(KM^3 + KQ_s M^2 + N_D M^2), \quad (51)$$

where $Q_s = \mathcal{O}(M)$ is the number of grid points used to search the pseudo-spectrum in (44). The complexity of SCVBI is upper bounded by [17]

$$\mathcal{O}(KMNT_p + M^3). \quad (52)$$

With the compact position grid of Q_k points for user k , the complexity of the EM-Turbo-BiSVBI is

$$\begin{aligned} \mathcal{O} \left(\left(\sum_{k=1}^K Q_k + 1 \right) MN (T_p + T_d) + |\hat{\mathcal{S}}|^3 \right. \\ \left. + \sum_{t_d=1}^{T_d} \sum_{n=1}^N \left(M |\mathcal{K}_{t_d,n}^d|^2 + |\mathcal{K}_{t_d,n}^d|^3 \right) \right). \end{aligned} \quad (53)$$

Therefore, the complexity of the overall algorithm is upper bounded by the summation of (51) - (53), which is much smaller than that of the original EM-Turbo-BiSVBI in (42).

VI. SIMULATIONS

In this section, we demonstrate the advantages of the proposed algorithm by comparison with the following baselines.

- **Variational Bayes' joint channel estimation and symbol decoding (VB-CESD) [14], [15]:** It is the state-of-the-art method for joint angular-delay domain channel estimation and data recovery.
- **ST-MUSIC [16]:** Use ST-MUSIC to estimate the angles and delays of channel paths, least square (LS) to estimate the channel gain, and MMSE to estimate the data.
- **Two-stage framework [10]:** In stage 1, use the SCVBI algorithm to estimate the location-domain channels; in stage2, use MMSE to estimate the data.
- **EM-Turbo-BiSVBI IID:** It is the proposed EM-Turbo-BiSVBI algorithm with an i.i.d. prior (the factor graph has no joint support vector \bar{s} and the elements of different s_k 's are i.i.d.).
- **EM-Turbo-BiVBI:** This scheme is a minor variation of the proposed scheme. The only difference is that it

directly calculates the posterior mean $\mu_\alpha = \mathbf{W}_\alpha^{-1} \mathbf{b}_\alpha$ using the high-dimensional matrix inverse instead of the subspace constrained matrix inverse.

- **Genie-aided:** It is the proposed method when the user locations and time offsets are perfectly known.

In the simulations, the BS is equipped with a UPA consisting of $M_x = 8$ horizontal antennas and $M_z = 8$ vertical antennas, for a total of $M = 64$ antennas. The number of OFDM subcarriers is $N = 1024$, the carrier frequency is 3.5 GHz, and the subcarrier interval is $f_0 = 30$ kHz. The users are divided into groups of similar positions and each user group is assigned with the same set of data subcarriers. In the simulations, we focus on a reference user group containing 4 users. There are $T_p = 1$ pilot OFDM symbol and $T_d = 2$ data OFDM symbols. The N^p pilot signals for each user are generated with random phase under the unit power constraint, and they are uniformly inserted in the N subcarriers without intersections. All users share the same N^d data subcarriers which are uniformly inserted in the N subcarriers to enjoy the frequency diversity gain. Moreover, the data signals for each user are generated by a complex Gaussian distribution with zero mean and unit variance. In the simulations, we fix $N^d = 256$ and vary N^p to show the effect of the number of pilot subcarriers on the performance.

The scatterers are distributed in a $100 \text{ m} \times 100 \text{ m} \times 10 \text{ m}$ area. The BS is at coordinates $[0 \text{ m}, 0 \text{ m}, 0 \text{ m}]^T$ and the mobile users are random distributed around coordinates $[100 \text{ m}, 0 \text{ m}, 0 \text{ m}]^T$ with the k -th user position denoted as $\mathbf{p}_{u,k} = [p_{u,k}^x, p_{u,k}^y, 0]^T$ in Cartesian coordinate system. We assume that the prior distribution of \mathbf{p}_u is $p^x \sim \mathcal{N}(p_{u,k}^x, \sigma_p^2/2)$ and $p^y \sim \mathcal{N}(p_{u,k}^y, \sigma_p^2/2)$, where σ_p^2 is set as 1. The channel is generated according to the UMA scenario in the Quadriga model defined by 3GPP R16 specifications [28].

The time offsets $\tau_{o,k}$'s are within $[-\frac{2}{B}, \frac{2}{B}]$, where $B = Nf_0$ denotes the total bandwidth. The number of azimuth and elevation angle grid points is set to $Q_1 = Q_2 = 16$ and the number of range grid points is set to $Q_r = 10$. We use the root mean square error (RMSE) as the performance metric for scatterer localization and the normalized mean square error (NMSE) as the performance metric for channel estimation and data recovery.

A. Convergence Behavior

In Fig. 5 and Fig. 6, we compare the convergence behavior of different schemes when the signal to noise ratio (SNR) is set to -5 dB and N^p is set to 8. The two-stage scheme converges very quickly but converges to a relative poor stationary point. In contrast, other schemes based on joint estimation converge within 25 iterations and they find better stationary solutions than the two-stage scheme. Moreover, both the convergence speed and steady-state performance of the proposed EM-Turbo-BiSVBI are similar to those of the more complicated EM-Turbo-BiVBI, which means that the subspace constrained matrix inverse approach can effectively reduce the computation overhead without performance degradation.

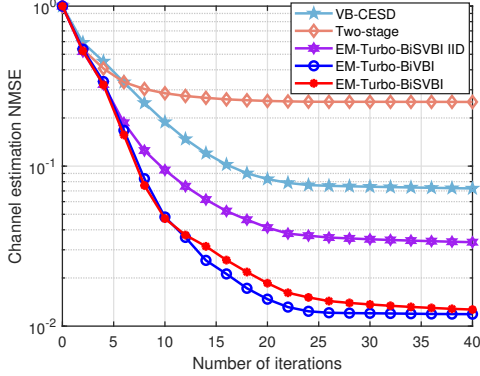


Figure 5: Convergence Behavior: Channel estimation NMSE versus the EM iteration number.

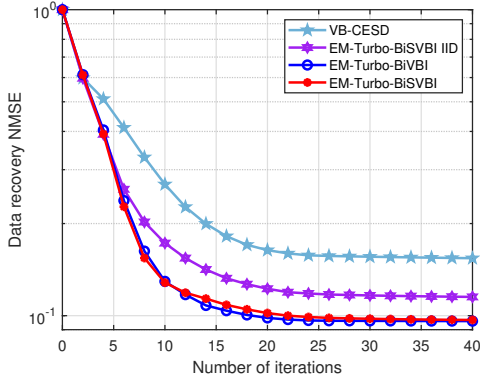


Figure 6: Convergence Behavior: Data recovery NMSE versus the EM iteration number.

B. Impact of SNR

In Fig. 7a, Fig. 7b, and Fig. 7c, we set $N^p = 8$ and evaluate the channel estimation NMSE, data recovery NMSE, and scatterer localization RMSE performance under different SNRs.³ It is obvious that the performance of all the schemes improves as SNR increases. The ST-MUSIC scheme works very poorly since the estimation error of delays is relatively large when the number of pilot subcarriers is small. Besides, the joint estimation schemes achieve a significant performance gain over the two-stage scheme. This is because channel estimation and data recovery can be mutually enhanced based on both received pilot and data signals. The EM-Turbo-BiSVBI IID scheme works better than the VB-CESD scheme, which reflects the advantage of position-domain channel modeling. Moreover, the performance gap between the EM-Turbo-BiSVBI and EM-Turbo-BiSVBI IID is significant, which means that the proposed three-layer BGG prior model can fully exploit the joint sparsity of MU channels to enhance the sensing/estimation performance. Finally, the performance of the proposed scheme is close to that of the genie-aided scheme, especially in terms of data recovery NMSE and scatterer localization RMSE, which implies that the non-ideal factors

³Since the VR-CESD and TS-MUSIC schemes estimate angles and delays of channel paths directly, we do not plot the scatterer localization RMSE performance for them.

can be estimated accurate enough by the Turbo-BiSVBI-M step.

C. Impact of Number of Pilot Subcarriers

In Fig. 8a, Fig. 8b, and Fig. 8c, we vary N^p from 2 to 32 to show how the number of pilot subcarriers affects the sensing/estimation performance when SNR = -5 dB. The proposed EM-Turbo-BiSVBI achieves the best performance among all the schemes. Besides, we find that the scatterer localization performance of the proposed EM-Turbo-BiSVBI is not sensitive to the number of pilot subcarriers. Even when $N^p = 2$, its localization RMSE is still very small. In other words, the proposed scheme can provide high-accuracy localization service with very little pilot subcarriers or even without any pilot.

VII. CONCLUSION

This paper propose a novel joint sensing and data recovery algorithm for massive MIMO-OFDM ISAC systems. A 3D location-domain sparse prior model is firstly introduced to capture the joint sparsity of the MU channel. Then, the joint problem is formulated as a bilinear structured sparse recovery problem with a dynamic position grid and imperfect parameters. An EM-Turbo-BiSVBI algorithm is proposed to solve this joint sensing and data recovery problem, where the E-step performs Bayesian estimation of the location-domain sparse MU channel by exploiting the joint sparsity, and the M-step refines the dynamic position grid and learns the imperfect factors via gradient update. In particular, a BiSVBI algorithm is proposed to solve the bilinear sparse inference problem in the E-step with both theoretical convergence guarantee and low complexity. In addition, an SMUSIC-SCVBI algorithm is proposed in the coarse estimation stage to narrow down the search range and reduce the effective dimension of the location-domain channel, which further reduces the complexity caused by the ultra-high-dimensional sparse channel in the entire 3D space. The proposed algorithm is shown by simulations to achieve much better trade-off between performance and complexity than various baseline algorithms.

APPENDIX

A. Proof of Lemma 2

Given $q(\mathbf{x}), q(\boldsymbol{\rho}), q(\mathbf{s}), q(\kappa)$, the KLD can be calculated as

$$\begin{aligned}
 \text{KL}(q \parallel p) &= \int q(\mathbf{v}) \ln \frac{q(\mathbf{v})}{\hat{p}(\mathbf{v} \mid \mathbf{y})} d\mathbf{v} \\
 &= \langle \ln q(\boldsymbol{\alpha}) \rangle_{q(\boldsymbol{\alpha})} - \langle \ln \hat{p}(\mathbf{v}, \mathbf{y}) \rangle_{q(\mathbf{v})} + C_1 \\
 &= \langle \ln q(\boldsymbol{\alpha}) \rangle_{q(\boldsymbol{\alpha})} - \langle \ln p(\boldsymbol{\alpha} \mid \boldsymbol{\rho}) \rangle_{q(\boldsymbol{\alpha})q(\boldsymbol{\rho})} \\
 &\quad - \langle \ln p(\mathbf{y} \mid \boldsymbol{\alpha}, \mathbf{x}, \kappa) \rangle_{q(\boldsymbol{\alpha})q(\mathbf{x})q(\kappa)} + C_1, \\
 &= \langle \ln q(\boldsymbol{\alpha}) \rangle_{q(\boldsymbol{\alpha})} + \langle \boldsymbol{\alpha}^H \text{Diag}(\langle \boldsymbol{\rho} \rangle) \boldsymbol{\alpha} \rangle_{q(\boldsymbol{\alpha})} \\
 &\quad + \langle \kappa \rangle \left\langle \|\mathbf{y} - \mathbf{A}_{\alpha} \boldsymbol{\alpha}\|^2 \right\rangle_{q(\boldsymbol{\alpha})q(\mathbf{x})} + C_1, \quad (54)
 \end{aligned}$$

where C_1 is a constant. Based on the constraint in (23), Problem \mathcal{A}_{VBI} is equivalent to finding the optimal parameters

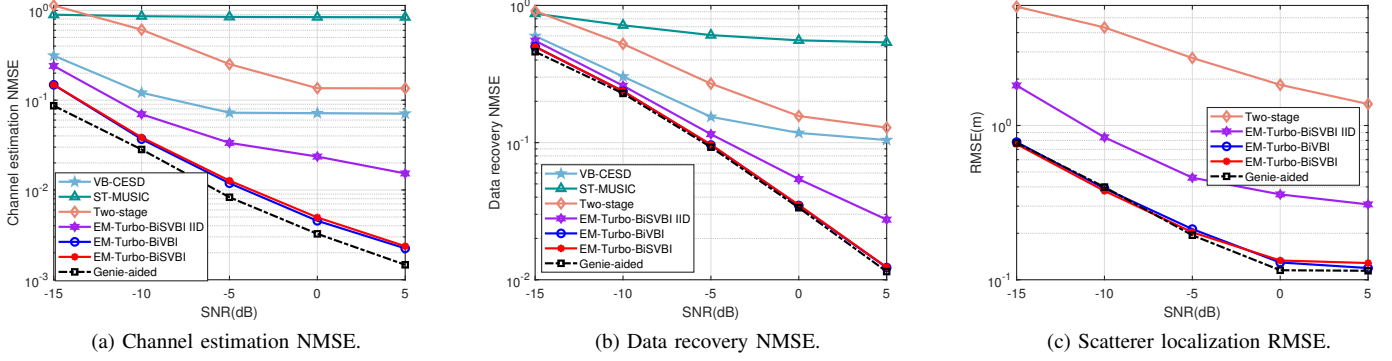


Figure 7: Sensing and estimation performance versus SNR.

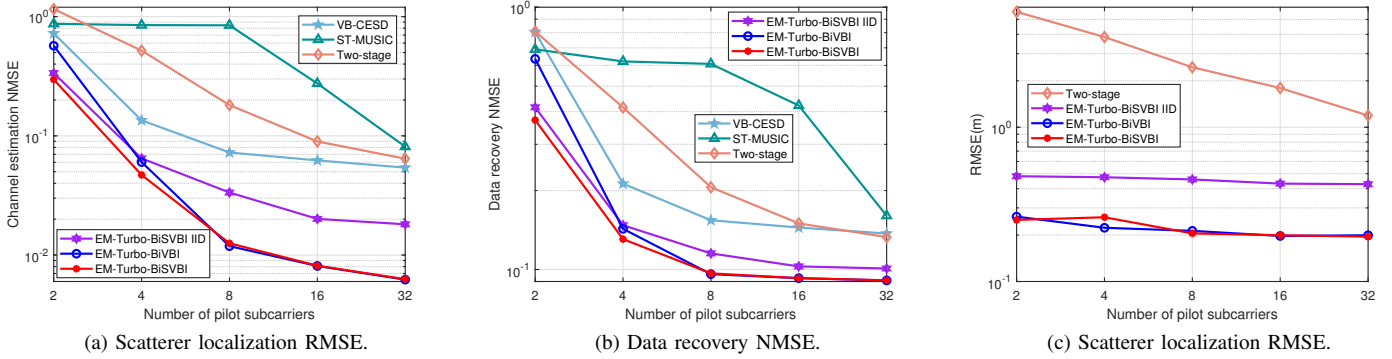


Figure 8: Sensing and estimation performance versus the number of pilot subcarriers.

of $q(\boldsymbol{\alpha})$, denoted by $\{\ddot{\mu}_{\alpha}, \ddot{\sigma}_{\alpha}^2\}$, so that the KLD in (54) is minimized. The equivalent optimization problem is formulated as

$$\begin{aligned} \ddot{\mu}_{\alpha}, \ddot{\sigma}_{\alpha}^2 &= \arg \min_{\boldsymbol{u}_{\alpha}, \boldsymbol{\sigma}_{\alpha}^2} \left[-\sum_{k=1}^K \sum_{q=0}^Q \ln \sigma_{\alpha, k, q}^2 - \boldsymbol{\mu}_{\alpha}^H \text{Diag}(1/\sigma_{\alpha}^2) \boldsymbol{\mu}_{\alpha} \right. \\ &\quad + \langle \boldsymbol{\alpha}^H (\mathbf{W}_{\alpha} - \text{Diag}(1/\sigma_{\alpha}^2)) \boldsymbol{\alpha} \rangle_{q(\boldsymbol{\alpha})} \\ &\quad \left. - \langle 2\Re \{ \boldsymbol{\alpha}^H (\mathbf{b}_{\alpha} - \text{Diag}(1/\sigma_{\alpha}^2) \boldsymbol{\mu}_{\alpha}) \} \rangle_{q(\boldsymbol{\alpha})} \right] \\ &= \arg \min_{\boldsymbol{u}_{\alpha}, \boldsymbol{\sigma}_{\alpha}^2} \left[-\sum_{k=1}^K \sum_{q=0}^Q \ln \sigma_{\alpha, k, q}^2 - \boldsymbol{\mu}_{\alpha}^H \text{Diag}(1/\sigma_{\alpha}^2) \boldsymbol{\mu}_{\alpha} \right. \\ &\quad + \boldsymbol{\mu}_{\alpha}^H (\mathbf{W}_{\alpha} - \text{Diag}(1/\sigma_{\alpha}^2)) \boldsymbol{\mu}_{\alpha} \\ &\quad + \text{Tr}((\mathbf{W}_{\alpha} - \text{Diag}(1/\sigma_{\alpha}^2)) \text{Diag}(\boldsymbol{\sigma}_{\alpha}^2)) \\ &\quad \left. - 2\Re \{ \boldsymbol{\mu}_{\alpha}^H (\mathbf{b}_{\alpha} - \text{Diag}(1/\sigma_{\alpha}^2) \boldsymbol{\mu}_{\alpha}) \} \right] \\ &= \arg \min_{\boldsymbol{u}_{\alpha}, \boldsymbol{\sigma}_{\alpha}^2} \left[\boldsymbol{\mu}_{\alpha}^H \mathbf{W}_{\alpha} \boldsymbol{\mu}_{\alpha} - 2\Re \{ \boldsymbol{\mu}_{\alpha}^H \mathbf{b}_{\alpha} \} \right. \\ &\quad \left. + \sum_{k=1}^K \sum_{q=0}^Q (\mathbf{W}_{\alpha, k, q} \sigma_{\alpha, k, q}^2 - \ln \sigma_{\alpha, k, q}^2) \right], \end{aligned} \quad (55)$$

which is equal to (26).

Similarly, given $q(\boldsymbol{\alpha}), q(\boldsymbol{\rho}), q(\boldsymbol{s}), q(\boldsymbol{\kappa})$, the KLD can be

calculated as

$$\begin{aligned} \text{KL}(q \parallel p) &= \langle \ln q(\mathbf{x}) \rangle_{q(\mathbf{x})} - \langle \ln p(\mathbf{x}) \rangle_{q(\mathbf{x})} \\ &\quad - \langle \ln p(\mathbf{y} \mid \boldsymbol{\alpha}, \mathbf{x}, \boldsymbol{\kappa}) \rangle_{q(\boldsymbol{\alpha})q(\mathbf{x})q(\boldsymbol{\kappa})} + C_2, \\ &= \sum_{t=1}^{T_d} \sum_{n=1}^N \left[\langle \ln q(\mathbf{x}_{t_d, n}) \rangle_{q(\mathbf{x}_{t_d, n})} \right. \\ &\quad + \langle \mathbf{x}_{t_d, n}^H \text{Diag}(\boldsymbol{\sigma}_{t_d, n}^2) \mathbf{x}_{t_d, n} \rangle_{q(\mathbf{x}_{t_d, n})} \\ &\quad \left. + \langle \boldsymbol{\kappa} \rangle \left\langle \|\mathbf{y}_{t_d, n}^d - \boldsymbol{\Psi}_n \mathbf{x}_{t_d, n}\|^2 \right\rangle_{q(\boldsymbol{\alpha})q(\mathbf{x}_{t_d, n})} \right] + C_2, \end{aligned} \quad (56)$$

where C_2 is a constant. Based on the constraint in (24), Problem \mathcal{A}_{VBI} is equivalent to finding the optimal parameters of $q(\mathbf{x})$, denoted by $\{\ddot{\mu}_{\mathbf{x}}, \ddot{\sigma}_{\mathbf{x}}^2\}$, so that the KLD in (54) is minimized. The equivalent optimization problem is formulated as

$$\begin{aligned} \ddot{\mu}_{x, t_d, n}, \ddot{\sigma}_{x, t_d, n}^2 &= \arg \min_{\boldsymbol{\mu}_{x, t_d, n}, \boldsymbol{\sigma}_{x, t_d, n}^2} \left[\boldsymbol{\mu}_{x, t_d, n}^H \mathbf{W}_{x, t_d, n} \boldsymbol{\mu}_{x, t_d, n} - 2\Re \{ \boldsymbol{\mu}_{x, t_d, n}^H \mathbf{b}_{x, t_d, n} \} \right. \\ &\quad \left. + \sum_{k \in \mathcal{K}_{t_d, n}^d} (\mathbf{W}_{x, t_d, k, n} \boldsymbol{\sigma}_{x, t_d, k, n}^2 - \ln \boldsymbol{\sigma}_{x, t_d, k, n}^2) \right], \end{aligned} \quad (57)$$

which is equal to (27).

B. Proof of Theorem 3

The BiSVBI algorithm can be viewed as an alternating optimization method to solve Problem \mathcal{A}_{VBI} . It is clear that the BiSVBI can monotonically decreasing the KLD objective, thus the KLD will converge to a limit. For convenience, we use

$$\boldsymbol{\xi} \triangleq \{\boldsymbol{\mu}_\alpha, \sigma_\alpha^2, \boldsymbol{\mu}_x, \sigma_x^2, \check{a}_{k,q}, \check{b}_{k,q}, \check{\lambda}_{k,q}, \check{c}, \check{d} \mid \forall k, q\}$$

to represent the parameters of $q(\mathbf{v})$. Let $\boldsymbol{\xi}_j$ denote the j -th block of $\boldsymbol{\xi}$ for $j = 1, \dots, B$, where $B = |\boldsymbol{\xi}|$. Then, the KLD in (21) can be rewritten as a function of $\boldsymbol{\xi}$, i.e.

$$\text{KL}(\boldsymbol{\xi}) = \int q(\mathbf{v}; \boldsymbol{\xi}) \ln \frac{q(\mathbf{v}; \boldsymbol{\xi})}{\hat{p}(\mathbf{v} \mid \mathbf{y}; \boldsymbol{\xi})} d\mathbf{v}. \quad (58)$$

In the following, we will prove that every limiting point $q^*(\mathbf{v}; \boldsymbol{\xi}^*)$ generated by the BiSVBI is a stationary solution of Problem \mathcal{A}_{VBI} .

In the t -th iteration of the BiSVBI, we update $\boldsymbol{\xi}_j, \forall j$ alternatively as

$$\boldsymbol{\xi}_j^{(t)} = \begin{cases} \text{argmin}_{\boldsymbol{\xi}_j} \text{KL}(\boldsymbol{\xi}_j, \boldsymbol{\xi}_{-j}^{(t-1)}), & \text{if } \boldsymbol{\xi}_j \neq \boldsymbol{\mu}_\alpha, \\ \boldsymbol{\mu}_\alpha^{(t)(B_\alpha)}, & \text{if } \boldsymbol{\xi}_j = \boldsymbol{\mu}_\alpha, \end{cases} \quad (59)$$

where $(\cdot)^{(t)}$ stands for the t -th iteration, $\boldsymbol{\xi}_{-j}^{(t-1)} = (\boldsymbol{\xi}_1^{(t)}, \dots, \boldsymbol{\xi}_{j-1}^{(t)}, \boldsymbol{\xi}_{j+1}^{(t-1)}, \dots, \boldsymbol{\xi}_B^{(t-1)})$, and $\boldsymbol{\mu}_\alpha^{(t)(B_\alpha)}$ is computed by the following gradient update for B_α times:

$$\begin{aligned} \boldsymbol{\mu}_\alpha^{(t)(i)} &= \boldsymbol{\mu}_\alpha^{(t)(i-1)} - \epsilon_\alpha^{(t)(i)} \nabla_{\boldsymbol{\mu}_\alpha} \text{KL}(\boldsymbol{\mu}_\alpha, \boldsymbol{\xi}_{-j}^{(t-1)}) \mid_{\boldsymbol{\mu}_\alpha = \boldsymbol{\mu}_\alpha^{(t)(i-1)}} \\ &= \boldsymbol{\mu}_\alpha^{(t)(i-1)} - \epsilon_\alpha^{(t)(i)} \nabla_{\boldsymbol{\mu}_\alpha} \varphi_\alpha(\boldsymbol{\mu}_\alpha) \mid_{\boldsymbol{\mu}_\alpha = \boldsymbol{\mu}_\alpha^{(t)(i-1)}}, \end{aligned} \quad (60)$$

for $i = 1, \dots, B_\alpha$, where $\epsilon_\alpha^{(t)(i)}$ is the step size determined by the Armijo rule. Based on the robust design, the initial value $\boldsymbol{\mu}_\alpha^{(t)(0)}$ is given by

$$\boldsymbol{\mu}_\alpha^{(t)(0)} = \begin{cases} \boldsymbol{\mu}_\alpha^{(t-1)}, & \text{if } \varphi(\boldsymbol{\mu}_{\alpha, \hat{\mathcal{S}}}^s) \geq \varphi(\boldsymbol{\mu}_\alpha^{(t-1)}), \\ \boldsymbol{\mu}_{\alpha, \hat{\mathcal{S}}}^s, & \text{otherwise.} \end{cases} \quad (61)$$

where $\boldsymbol{\mu}_{\alpha, \hat{\mathcal{S}}}^s$ is obtained by the subspace constrained matrix inverse in (29). The robust design in (61) can ensure $\text{KL}(\boldsymbol{\mu}_\alpha^{(t-1)}, \boldsymbol{\xi}_{-j}^{(t-1)}) \geq \text{KL}(\boldsymbol{\mu}_\alpha^{(t)(0)}, \boldsymbol{\xi}_{-j}^{(t-1)})$, where the equality holds when $\varphi(\boldsymbol{\mu}_{\alpha, \hat{\mathcal{S}}}^s) \geq \varphi(\boldsymbol{\mu}_\alpha^{(t-1)})$. Besides, the gradient update in (60) can ensure $\text{KL}(\boldsymbol{\mu}_\alpha^{(t)(i-1)}, \boldsymbol{\xi}_{-j}^{(t-1)}) \geq \text{KL}(\boldsymbol{\mu}_\alpha^{(t)(i)}, \boldsymbol{\xi}_{-j}^{(t-1)}), \forall i$, where the equality holds only when the gradient w.r.t. $\boldsymbol{\mu}_\alpha$ is zero. Based on these, we have

$$\begin{aligned} \text{KL}(\boldsymbol{\mu}_\alpha^{(t-1)}, \boldsymbol{\xi}_{-j}^{(t-1)}) &\geq \text{KL}(\boldsymbol{\mu}_\alpha^{(t)(0)}, \boldsymbol{\xi}_{-j}^{(t-1)}) \geq \\ \text{KL}(\boldsymbol{\mu}_\alpha^{(t)(1)}, \boldsymbol{\xi}_{-j}^{(t-1)}) &\geq \dots \geq \text{KL}(\boldsymbol{\mu}_\alpha^{(t)(B_\alpha)}, \boldsymbol{\xi}_{-j}^{(t-1)}) \\ &= \text{KL}(\boldsymbol{\mu}_\alpha^{(t)}, \boldsymbol{\xi}_{-j}^{(t-1)}). \end{aligned} \quad (62)$$

Now we explain the non-increasing property of the KLD in the t -th iteration. For the case of $\boldsymbol{\xi}_j \neq \boldsymbol{\mu}_\alpha$, it is clear that $\text{KL}(\boldsymbol{\xi}_j, \boldsymbol{\xi}_{-j}^{(t-1)})$ is minimized w.r.t. $\boldsymbol{\xi}_j$. While for the case of $\boldsymbol{\xi}_j = \boldsymbol{\mu}_\alpha$, we have $\text{KL}(\boldsymbol{\mu}_\alpha^{(t-1)}, \boldsymbol{\xi}_{-j}^{(t-1)}) \geq \text{KL}(\boldsymbol{\mu}_\alpha^{(t)}, \boldsymbol{\xi}_{-j}^{(t-1)})$,

i.e., the KLD is non-increasing. Therefore, the KLD will keep decreasing until converging to a certain value, and we must have

$$\lim_{t \rightarrow \infty} \nabla_{\boldsymbol{\xi}_j} \text{KL}(\boldsymbol{\xi}_j, \boldsymbol{\xi}_{-j}^{(t-1)}) = 0, \forall j. \quad (63)$$

Otherwise, the KLD will keep decreasing to negative infinity, which contradicts with the fact that $\text{KL}(\boldsymbol{\xi}) \geq 0$. Then according to (63) and the property of gradient update, we must have $\lim_{t \rightarrow \infty} \|\boldsymbol{\mu}_\alpha^{(t)} - \boldsymbol{\mu}_\alpha^{(t-1)}\| = 0$. Moreover, it follows from (63) and the strong convexity of $\text{KL}(\boldsymbol{\xi}_j, \boldsymbol{\xi}_{-j}^{(t-1)})$ w.r.t. $\boldsymbol{\xi}_j, \forall \boldsymbol{\xi}_j \neq \boldsymbol{\mu}_\alpha$ that $\lim_{t \rightarrow \infty} \|\boldsymbol{\xi}_j^{(t)} - \boldsymbol{\xi}_j^{(t-1)}\| = 0, \forall \boldsymbol{\xi}_j \neq \boldsymbol{\mu}_\alpha$. Therefore, we have

$$\lim_{t \rightarrow \infty} \|\boldsymbol{\xi}_j^{(t)} - \boldsymbol{\xi}_j^{(t-1)}\| = 0, \forall j. \quad (64)$$

It follows from (64) that all the B sequences $\{\boldsymbol{\xi}_j^{(t)}, \boldsymbol{\xi}_{-j}^{(t)}\}, j = 1, \dots, B$ have the same set of limiting points. Let $\{\boldsymbol{\xi}_j^{(t_k)}, \boldsymbol{\xi}_{-j}^{(t_k)}, k = 1, 2, \dots\}$ denote a subsequence that converges to a limiting point $\boldsymbol{\xi}^*$. Suppose $\boldsymbol{\xi}^*$ is not a stationary point of $\text{KL}(\boldsymbol{\xi})$, then $\nabla_{\boldsymbol{\xi}} \text{KL}(\boldsymbol{\xi}) \neq 0$ and it follows from (64) that $\lim_{k \rightarrow \infty} \nabla_{\boldsymbol{\xi}_j} \text{KL}(\boldsymbol{\xi}_j, \boldsymbol{\xi}_{-j}^{(t_k)}) \neq 0$ must hold at least for some j , which contradicts with (63). Therefore, every limiting point $\boldsymbol{\xi}^*$ must be a stationary point of $\text{KL}(\boldsymbol{\xi})$. In other word, every limiting point $q^*(\mathbf{v}; \boldsymbol{\xi}^*)$ generated by the BiSVBI is a stationary solution of Problem \mathcal{A}_{VBI} .

REFERENCES

- [1] J. A. Zhang, F. Liu, C. Masouros, R. W. Heath, Z. Feng, L. Zheng, and A. Petropulu, "An overview of signal processing techniques for joint communication and radar sensing," *IEEE J. Sel. Topics Signal Process.*, vol. 15, no. 6, pp. 1295–1315, 2021.
- [2] F. Liu, Y. Cui, C. Masouros, J. Xu, T. X. Han, Y. C. Eldar, and S. Buzzi, "Integrated sensing and communications: Toward dual-functional wireless networks for 6G and beyond," *IEEE J. Sel. Areas Commun.*, vol. 40, no. 6, pp. 1728–1767, 2022.
- [3] F. Liu, C. Masouros, A. P. Petropulu, H. Griffiths, and L. Hanzo, "Joint radar and communication design: Applications, state-of-the-art, and the road ahead," *IEEE Trans. Commun.*, vol. 68, no. 6, pp. 3834–3862, 2020.
- [4] A. Liu, Z. Huang, M. Li, Y. Wan, W. Li, T. X. Han, C. Liu, R. Du, D. K. P. Tan, J. Lu, Y. Shen, F. Colone, and K. Chetty, "A survey on fundamental limits of integrated sensing and communication," *IEEE Commun. Surveys Tuts.*, vol. 24, no. 2, pp. 994–1034, 2022.
- [5] X. Rao and V. K. N. Lau, "Distributed compressive CSIT estimation and feedback for FDD multi-user massive MIMO systems," *IEEE Trans. Signal Process.*, vol. 62, no. 12, pp. 3261–3271, 2014.
- [6] A. Liu, F. Zhu, and V. K. N. Lau, "Closed-loop autonomous pilot and compressive CSIT feedback resource adaptation in multi-user FDD massive MIMO systems," *IEEE Trans. Signal Process.*, vol. 65, no. 1, pp. 173–183, 2017.
- [7] Z. Huang, K. Wang, A. Liu, Y. Cai, R. Du, and T. X. Han, "Joint pilot optimization, target detection and channel estimation for integrated sensing and communication systems," *IEEE Trans. Wireless Commun.*, 2022, doi: 10.1109/TWC.2022.3183621.
- [8] W. Xu, Y. Xiao, A. Liu, and M. Zhao, "Joint scattering environment sensing and channel estimation for integrated sensing and communication," in *Proc. IEEE Int. Conf. Commun. (ICC)*, May 2023, pp. 541–546.
- [9] W. Xu, Y. Xiao, A. Liu, M. Lei, and M.-J. Zhao, "Joint scattering environment sensing and channel estimation based on non-stationary Markov random field," *IEEE Trans. Wireless Commun.*, vol. 23, no. 5, pp. 3903–3917, 2024.
- [10] T. Cui and C. Tellambura, "Semiblind channel estimation and data detection for OFDM systems with optimal pilot design," *IEEE Trans. Commun.*, vol. 55, no. 5, pp. 1053–1062, 2007.
- [11] J. T. Parker, P. Schniter, and V. Cevher, "Bilinear generalized approximate message passing-part I: Derivation," *IEEE Trans. Signal Process.*, vol. 62, no. 22, pp. 5839–5853, 2014.

- [12] K. Ito, T. Takahashi, S. Ibi, and S. Sampei, "Bilinear gaussian belief propagation for large MIMO channel and data estimation," in *Proc. IEEE Global Commun. Conf. (GLOBECOM)*, Dec. 2020, pp. 1–6.
- [13] F. Steiner, A. Mezghani, L. Swindlehurst, J. A. Nossek, and W. Utschick, "Turbo-like joint data-and-channel estimation in quantized massive mimo systems," in *Proc. Int. ITG Workshop Smart Antennas*, 2016, pp. 1–5.
- [14] S. S. Thoota and C. R. Murthy, "Variational Bayes' joint channel estimation and soft symbol decoding for uplink massive MIMO systems with low resolution ADCs," *IEEE Trans. Commun.*, vol. 69, no. 5, pp. 3467–3481, 2021.
- [15] ———, "Massive MIMO-OFDM systems with low resolution ADCs: Cramér-rao bound, sparse channel estimation, and soft symbol decoding," *IEEE Trans. Signal Process.*, vol. 70, pp. 4835–4850, 2022.
- [16] Y.-Y. Wang, J.-T. Chen, and W.-H. Fang, "TST-MUSIC for joint DOA-delay estimation," *IEEE Trans. Signal Process.*, vol. 49, no. 4, pp. 721–729, 2001.
- [17] A. Liu, Y. Zhou, and W. Xu, "Subspace constrained variational Bayesian inference for structured compressive sensing with a dynamic grid," *IEEE Trans. Signal Process.*, pp. 1–15, 2025.
- [18] A. Liu, L. Lian, V. Lau, G. Liu, and M.-J. Zhao, "Cloud-assisted cooperative localization for vehicle platoons: A turbo approach," *IEEE Trans. Signal Process.*, vol. 68, pp. 605–620, 2020.
- [19] J. Hong, X. Yin, and Z. Yu, "Joint channel parameter estimation and scatterers localization," *IEEE Trans. Wireless Commun.*, pp. 1–1, 2022.
- [20] A. Liu, G. Liu, L. Lian, V. K. N. Lau, and M.-J. Zhao, "Robust recovery of structured sparse signals with uncertain sensing matrix: A Turbo-VBI approach," *IEEE Trans. Wireless Commun.*, vol. 19, no. 5, pp. 3185–3198, 2020.
- [21] F. Kschischang, B. Frey, and H.-A. Loeliger, "Factor graphs and the sum-product algorithm," *IEEE Trans. Inf. Theory*, vol. 47, no. 2, pp. 498–519, 2001.
- [22] D. G. Tzikas, A. C. Likas, and N. P. Galatsanos, "The variational approximation for Bayesian inference," *IEEE Signal Process. Mag.*, vol. 25, no. 6, pp. 131–146, 2008.
- [23] H. Duan, L. Yang, J. Fang, and H. Li, "Fast inverse-free sparse Bayesian learning via relaxed evidence lower bound maximization," *IEEE Signal Process. Lett.*, vol. 24, no. 6, pp. 774–778, 2017.
- [24] W. Xu, A. Liu, B. Zhou, and M.-j. Zhao, "Successive linear approximation VBI for joint sparse signal recovery and dynamic grid parameters estimation," [Online]. Available: <https://arxiv.org/pdf/2307.09149>.
- [25] J. A. Tropp and A. C. Gilbert, "Signal recovery from random measurements via orthogonal matching pursuit," *IEEE Trans. Inf. Theory*, vol. 53, no. 12, pp. 4655–4666, 2007.
- [26] M. Wax and I. Ziskind, "Detection of the number of coherent signals by the MDL principle," *IEEE Trans. Acoust. Speech Signal Process.*, vol. 37, no. 8, pp. 1190–1196, 1989.
- [27] X. Li and K. Pahlavan, "Super-resolution toa estimation with diversity for indoor geolocation," *IEEE Trans. Wireless Commun.*, vol. 3, no. 1, pp. 224–234, 2004.
- [28] 3GPP TR 38.901 *Channel Model*. Wiley 5G Ref, 2021.